XXIII. PLASMAS AND CONTROLLED NUCLEAR FUSION

A. Active Plasma Systems*

Academic and Research Staff

Prof. L. D. Smullin
Prof. A. Bers
Prof. R. J. Briggs
Prof. R. R. Parker

Graduate Students

R. R. Bartsch
S-L. Chou
J. A. Davis
G. W. Goddard
F. Herba
B. R. Kusse
R. K. Linford
J. A. Mangano
H. M. Schneider

RESEARCH OBJECTIVES

The Active Plasma Systems group will continue to focus its attention on phenomena in nonequilibrium plasmas. The theory of velocity-space-induced instabilities will continue to be refined, with more attention paid to geometries of finite, transverse, and axial dimensions.

Experiments will continue to be centered around the beam-plasma discharge, and will include studies of ion-cyclotron and lower-hybrid-resonance heating. The parametric behavior of the beam-plasma discharge will continue to be a principal focus of interest.

1. Studies of the Beam-Plasma Discharge

During the past year, an electrostatic analyzer was developed for measuring the axial energy of the ions escaping from the end of the discharge. "Parallel temperatures" of 5-10 eV are observed, and since these measurements are made just beyond the mirror peaks, one may assume at least an equal transverse temperature. With this analyzer in place, it will now be possible to make direct and continuous measurements of the escaping ion energy as a function of the system parameters: beam power, magnetic field, pulsed gas transient, ion-cyclotron heating, and so forth.

L. D. Smullin

2. Plasma Heating Experiment

Our primary purpose in this experiment is to heat the ions of our beam-plasma discharge and assess the effects of higher ion temperature on the character of the discharge. The basic method of heating will involve coupling of RF energy to the ions; however, the specifics are still uncertain. At present, it appears that the method of coupling will be either to appropriately design a distributed coupling structure or modulate the electron beam. The frequency will probably be in the neighborhood of the ion-cyclotron resonance frequency, but we shall also investigate the possibility of using the lower hybrid frequency, particularly with the beam-modulation method.

3. Studies of Ion Cyclotron Wave

In addition to the program that has as its main objective plasma heating, we plan to continue studies of ion-cyclotron wave propagation. This work would continue the work

*This work was supported by the National Science Foundation (Grant GK-1165).

that we have discussed in previous Quarterly Progress Reports and would utilize the techniques and methods already described. The specific problems that we would like to explore are the following.

Electron Landau-damping of the ion-cyclotron wave. Our theoretical calculations have shown that if the electrons do indeed interact with the wave to cause the observed damping on a collisionless basis, then significant departures from exponential damping should be observable.

The physical mechanisms responsible for the observed width of the ion resonance. The experimentally obtained dispersion and resonance curves can be predicted from our theoretical mode by inserting and adjusting a phenomenological damping term in the ion dielectric tensor. We hope to separate the effects of ion-neutral and ion-ion collisions and cyclotron damping by studying the behavior of the damping as a function of plasma density and neutral pressure.

Propagation and/or resonance effects at the harmonics of ω_{ci}. While observation of harmonic-resonance effects have been made, no detailed quantitative comparison with theory exists. We hope that if harmonic-resonance effects are observed, they can be quantitatively related to the ion temperature.

R. R. Parker

4. Nonadiabatic Trapping of an Ion Beam

An experimental investigation of the trapping of a spiralling ion beam by two-stream instability effects is planned. The Lithium ion beam (energy ~100 volts) will be derived from a commercially available solid ion emitter and injected with axial velocity opposite to a tenuous hollow electron beam.

R. J. Briggs

5. Beam Plasma Interactions: Experiments and Theory

We shall continue experiments to explore the interactions of a plasma with a beam that spirals across the magnetic field. Theoretical work has begun to describe the modes of beams with drift motion both along and across the magnetic field.

Computer simulation of the nonlinear beam-plasma interaction has been completed. We are continuing our computer studies of the plasma-vacuum boundary. The self-consistent effects of plasma density gradients and thermal motion will be studied. We are also investigating the effects of density gradients on the axial-propagation modes of a magnetized column.

During the coming year, we plan to initiate a study of nonlinear mode-mode couplings in plasmas and, in particular, beam-plasma systems, and the stability analysis of finite and inhomogeneous plasmas. We are now investigating various approaches to the problem of determining the effects of finite system length on the infinite-system stability criteria.

A. Bers, R. J. Briggs

1. BEAM-PLASMA DISCHARGE: SYSTEM D

Experiment

The axial extent of the discharge and the ratio of $T_{\parallel}/T_{\perp}$ for the high-energy electrons have been determined from the observed axial variation of the plasma diamagnetism during the beam-plasma discharge. Observations of low-frequency oscillations stimulated by a low-voltage electron beam in the afterglow have been extended.[1]

The diamagnetism of the plasma was observed with a 765-turn coil, 1/2 inch in diameter and 1 inch long, which was movable axially at a radius of ~3 1/2-4 inches. The observed density variation as interpreted from the diamagnetism is shown in Fig. XXIII-1 as a function of axial distance. The data have been corrected for the axial

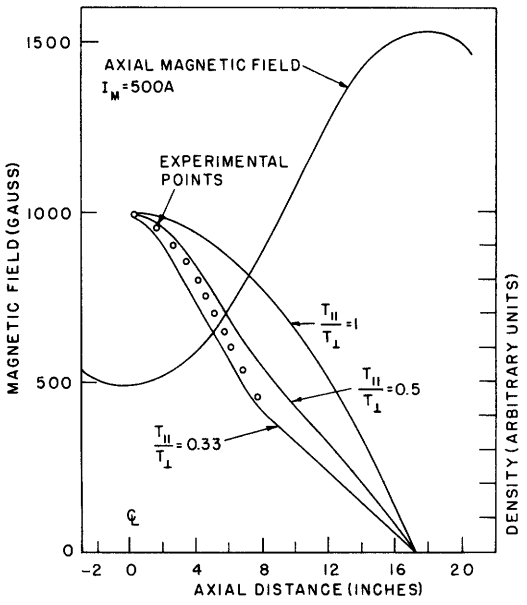

Fig. XXIII-1. Experimental density profile.

variation of the transverse energy and the variation of the outside boundary of the plasma. The density profile has been compared with Post's description of the axial density variation in a magnetic mirror system.[2] The axial variation is given by

$$n_e = n \frac{\psi t}{\psi - 1 + t} \frac{(1-\psi/R)^{1/2}}{(1-1/R)},$$

where n is the midplane density, ψ is the ratio of the magnetic field at a point in the system to its center line value, R is the mirror ratio, and t is $T_{\parallel}/T_{\perp}$, with $T_{\parallel}$ and $T_{\perp}$ being the parallel and perpendicular temperatures for a Maxwellian description of the plasma. The magnetic field profile and n_e for t = 0.33, 0.5, and 1 are shown in

Fig. XXIII-1. The ratio of parallel to longitudinal temperatures is observed to fall in the range 0.33-0.5. The hot-electron temperature has been previously measured to be in the range 10-14 keV. The plasma size is apparent from the profile shown in Fig. XXIII-1 where the end wall of the system is located at the peak of the magnetic mirror.

Low-frequency oscillations stimulated by a pulsed low-voltage beam in the afterglow have been observed on beam current pickups in the beam collector. The pickups are located at 90° to each other to determine the angular mode number of the oscillations. The low-level beam pulsewidth ($\lesssim$20 μsec) necessary to avoid interaction with the self-generated plasma requires the use of an oscilloscope to observe the oscillations. The variation of the frequency of the oscillations with delay time in the afterglow is shown in Fig. XXIII-2 where the frequency has been visually determined from photographs of

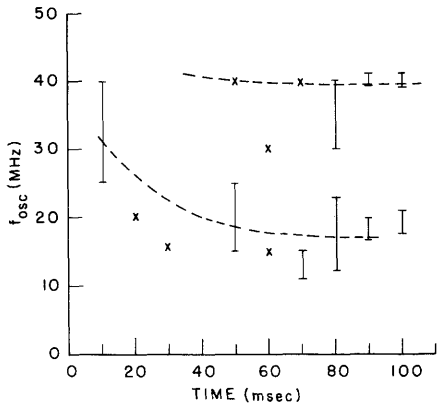

Fig. XXIII-2.
Oscillation frequency at times in the afterglow.

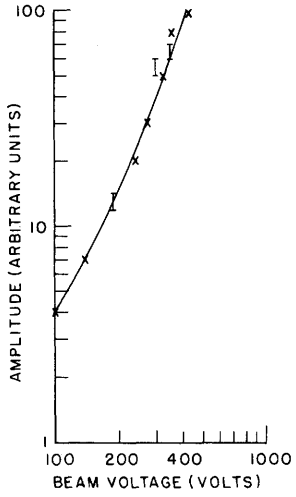

Fig. XXIII-3.
Amplitude of oscillations as a function of low-level beam voltage.

the oscillations. The variation of amplitude with beam voltage is shown in Fig. XXIII-3. The oscillations as observed on the two probes are found to be in phase (m = 0).

Model for Low-Frequency Oscillations

The parameters of the beam and plasma in System D indicate that the beam and plasma waves are in synchronism at a frequency just below the plasma frequency of the cold electrons. Oscillations at the cold-electron plasma frequency ($f \gtrsim 90$ mc) have been reported[3] and the interaction at synchronism explained for a plasma with both cold and hot electrons.[4] The model proposed for the observed oscillations ($f \sim 20$-50 mc) is that of the periodic field monotron discussed by Wesselberg.[5] The periodic field monotron consists of a resonant slow-wave structure and a zero space-charge beam.

Integration of the force equations for the beam particles reveals that the beam particles lose energy to the oscillation over certain ranges of the system parameters (transit angle, etc.). This has previously been studied in several limiting cases.[6,7] Numerical integration of the force equations used by Jepson in the limiting case of $\omega L/v_{beam} \ll 1$ has yielded the results obtained by Wesselberg for the zero-space case (arbitrary $\omega L/v_o$). An energy-loss contour for an electric field of the form

$$E_z = 0.1\left(\frac{mv_b^2}{2eL}\right)\cos kz \qquad 0 \leq z \leq L$$

is shown in Fig. XXIII-4. Other bands are indicated in the regions of frequency when the bands cross $k = n\pi/L$, $n = 1, 2, 3$. The energy loss per beam particle is observed to peak at $k = n\pi/L$.

The plasma cavity system has been studied to determine the existence of

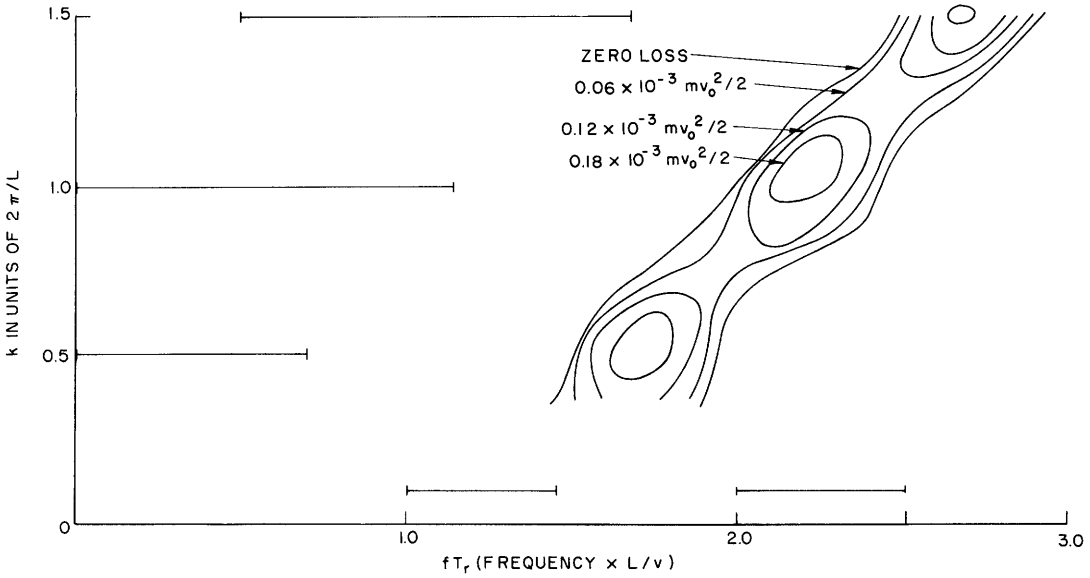

Fig. XXIII-4. Energy loss contours in standing-wave field.

low-frequency resonances. The lossless plasma waves in an infinitely long cylindrical waveguide can be described by the following quasi-static dispersion relation in the range of parameters

$$\omega_{ci} \ll \omega_{pi},\ \omega \ll \omega_{pe\ cold},\ \omega_{pe\ hot} \ll \omega_{ce},$$

by using the transport model for the hot electrons.

$$p^2\left(1-\frac{\omega_{pi}^2}{\omega^2}\right)+k^2\left(1-\frac{\omega_{pe\ cold}^2}{\omega^2}\right)+\frac{\omega_{pe\ hot}^2}{V_T^2}=0.$$

A field of the form $\phi=\frac{E_{zo}}{k}\sin kz\,J_o(pr)$ has been used. The $k(\omega)$ for a typical plasma parameters diagram is given in Fig. XXIII-5. The beam waves are indicated for $k_b=\omega/v_o$. If the system is assumed to be L long and we require $E_r=0$ at the end walls,

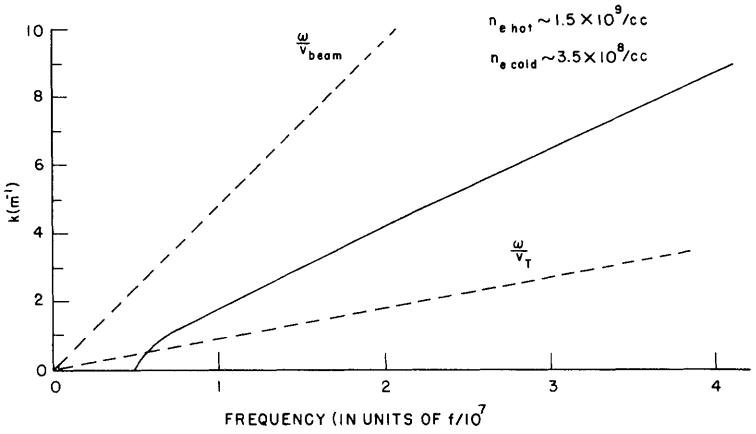

Fig. XXIII-5. Lossles $k(\omega)$.

we find that the plasma cavity system has resonances at $k_n=n\pi/L$ and

$$\omega_n=\sqrt{\frac{p^2\omega_{pi}^2+k_n^2\omega_{pe\ cold}^2}{p^2+k_n^2+\omega_{pe\ hot}^2/V_T^2}}.$$

Analysis of the possible loss mechanisms indicates that for the range of parameters of the System D afterglow, Landau damping is the most significant loss mechanism for the infinitely long, uniformly filled cylindrical plasma waveguide. $k(\omega_{real})$ and $\omega(k_{real})$ are given in Fig. XXIII-6 for a typical set of plasma parameters. The dispersion relation[8] is given below

$$0=p^2\left(1-\frac{\omega_{pi}^2}{\omega^2}\right)+k^2\left[1-\frac{\omega_{pe\ cold}^2}{\omega^2}+\frac{\omega_{pe\ hot}^2}{k^2V_T^2}\left(1+\frac{\omega}{\sqrt{2}\,kV_T}Z\left(\frac{\omega}{\sqrt{2}\,kV_T}\right)\right)\right],$$

where it has been assumed that $pV_T/\omega c \ll 1$.

The effects of a nonfilled cavity, both radially and axially, and the effects of finite

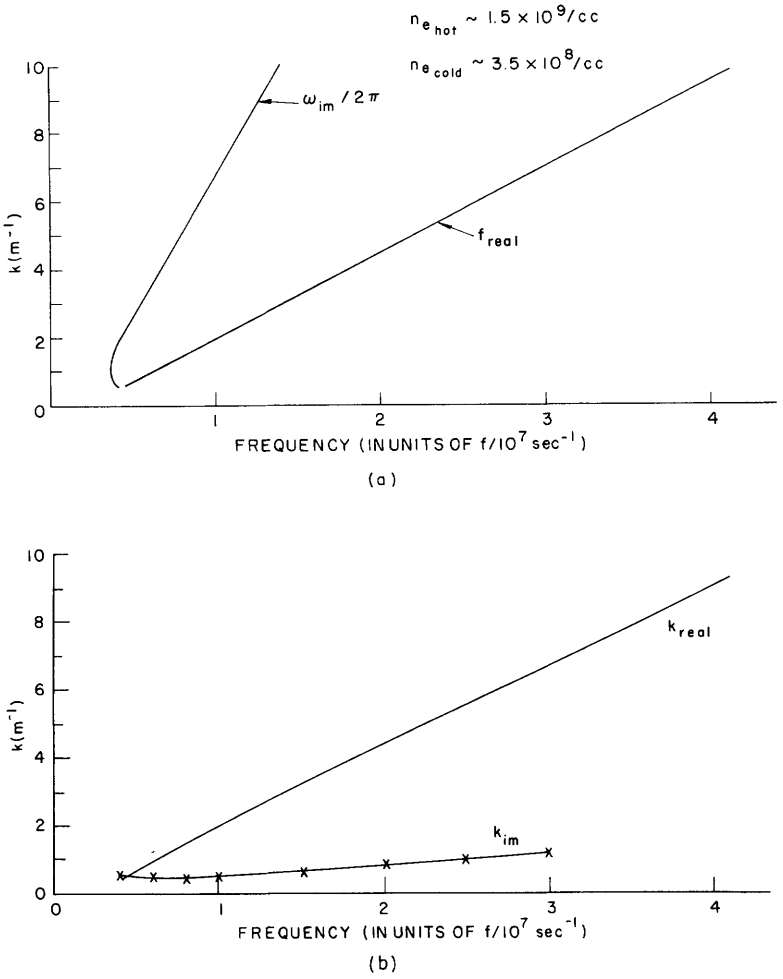

Fig. XXIII-6.
(a) Complex frequency for real wave number with Landau damping.
(b) Complex wave number for real frequency with Landau damping.

system length on the Landau-damping model are now being investigated to determine whether the beam energy loss to the oscillations is sufficient to overcome the plasma losses.

The author wishes to acknowledge the use of the facilities of the Francis Bitter National Magnet Laboratory for the experiments reported here, and the use of the facilities of Project MAC for the computations.

R. R. Bartsch

References

1. R. R. Bartsch, "Beam-Plasma Discharge: System D," Quarterly Progress Report No. 86, Research Laboratory of Electronics, M.I.T., July 15, 1967, p. 146.
2. R. F. Post, "Velocity-Space Instabilities in the Mirror Machine," Risö Report No. 18, Danish Atomic Energy Commission, Research Establishment at Risø, Physics Department, "International Summer Course in Plasma Physics," November 1960, see pp. 217-222.
3. R. R. Bartsch, op. cit., pp. 143-146.

4. S. L. Chou, "Electron Beam Interactions with Ions in a Plasma," S.M. Thesis, Department of Electrical Engineering, M.I.T., September 1967.

5. T. Wesselberg, "A General Theory of Klystrons with Arbitrary Extended Interaction Fields," Report No. 376, Microwave Laboratory, Stanford University, March 1957.

6. R. L. Jepsen, "Ion Oscillations in Electron Beam Tubes; Ion Motion and Energy Transfer," Proc. IRE 45, 1069-1080 (1957).

7. J. Marcum, "Interchange of Energy Between an Electron Beam and an Oscillating Electric Field," J. Appl. Phys. 17, 4-11 (1946).

8. A. Bers, "Theory of Beam-Plasma Interactions," Quarterly Progress Report No. 85, Research Laboratory of Electronics, M.I.T., April 15, 1967, pp. 163-164.

2. SPIRALING BEAM-PLASMA INTERACTIONS

Experimental Observations

Oscillations near the electron cyclotron frequency ω_{ce} and its harmonics, observed in the spiraling beam-plasma experiment, have been discussed in a previous report.[1] Oscillations have been observed above ω_{ce}, $2\omega_{ce}$ and $3\omega_{ce}$ which scaled with the magnetic field. Recently, azimuthal wavelength measurements of these signals have been made, and they will be discussed in this report. In all of the following observations a continuously flowing, spiraling electron beam was used.

Three radial electric monopoles were placed 90° apart, azimuthally around the stainless-steel screen that surrounds the discharge region (see Fig. XXIII-7). They

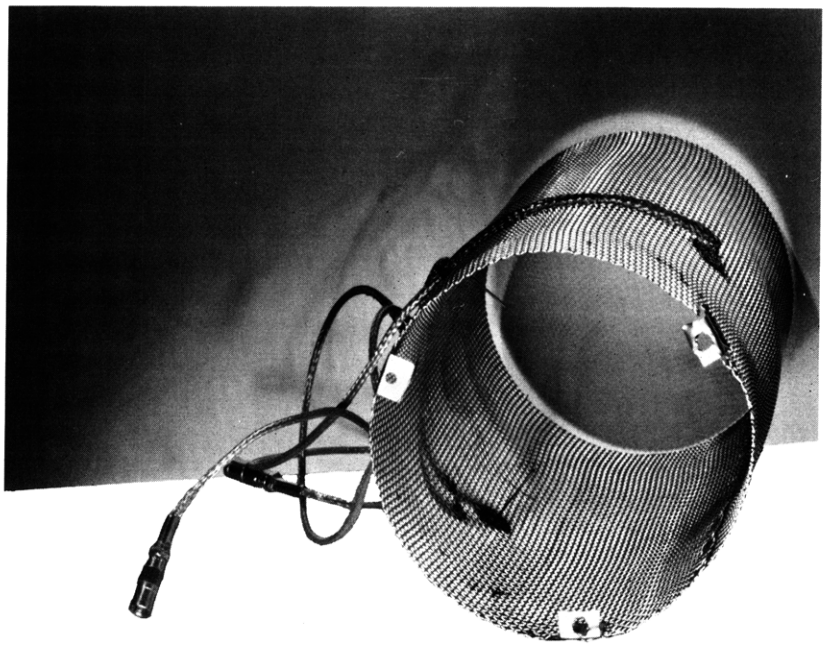

Fig. XXIII-7. Azimuthal probes.

were located 4 inches from the gun and 2 inches from the collector, and were approximately 0.75 inch long. Shielded cables carried the signals from these probes to a dual-beam oscilloscope. One signal was used to trigger both beams and was displayed on the upper trace. A second signal was displayed on the lower beam and the relative phase between the two signals was observed.

Figure XXIII-8 shows the results when a 62.5-mHz signal that was between ω_{ce} and $2\omega_{ce}$ was observed. The two traces shown in Fig. XXIII-8a were from signals on probes 90° apart. The traces in Fig. XXIII-8b were from signals on probes 180° apart. Under the assumption of an $e^{jm\theta}$ dependence, these results indicate an m = 1 mode.

Similar observations were made on an oscillation above $2\omega_{ce}$ and below $3\omega_{ce}$. They indicated that this was an m = 2 mode. Reversing the direction of the magnetic field

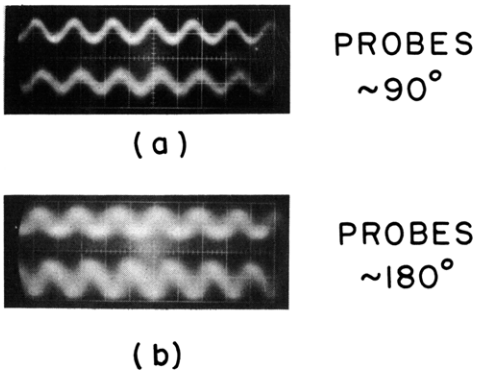

Fig. XXIII-8.

Azimuthal phase variation of m = 0 mode. (a) Probes, 90°. (b) Probes, 180°.

resulted in a change in the sign of m.

Measurements have also been made of the frequency dependence on beam density. The beam current and beam voltage can be controlled independently. The following observations were made at a constant beam voltage and constant magnetic field. The beam current was varied continuously from 0 to 10 mA, and the signal on one of the

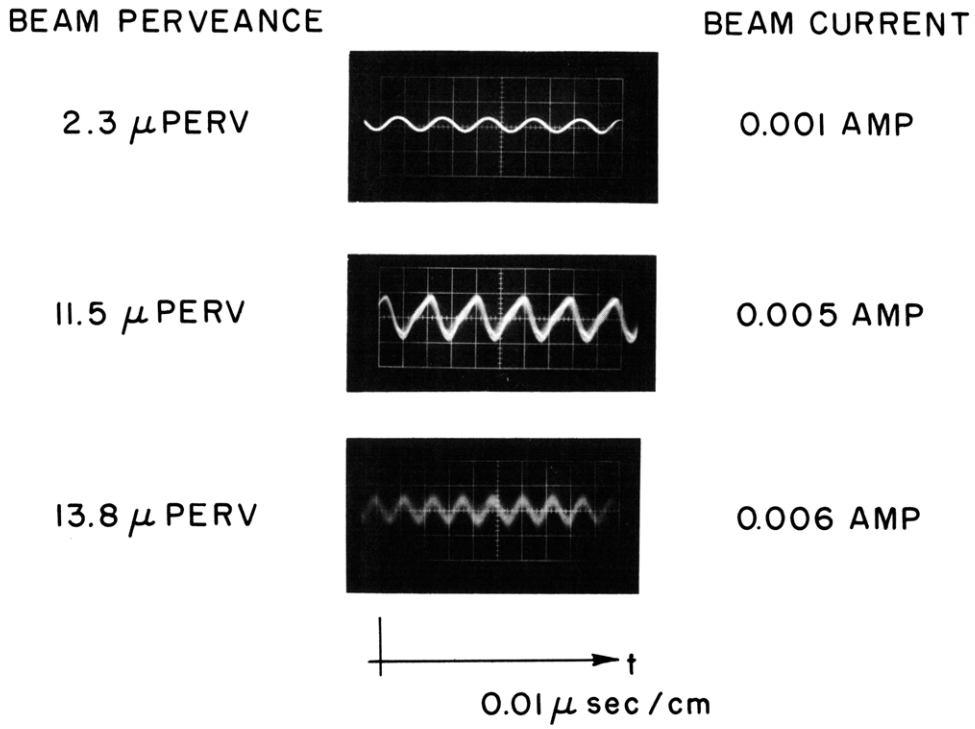

Fig. XXIII-9. Dependence of mode number m on beam density.

radial field probes was observed on an oscilloscope. Three characteristic waveforms and their corresponding beam currents are shown in Fig. XXIII-9. It can be seen that a 1-mA beam resulted in oscillations at the m = 1 mode only. The waveform was essentially a pure sinusoid. As the beam current was increased to 5 mA the m = 1 and m = 2 modes were observed. At 6 mA the m = 1 mode could no longer be seen. The signal was no longer a sinusoid, but appeared to be composed of m = 2 and higher modes.

These results indicate that the higher m-modes are present with higher beam densities. Since the plasma is created by the beam, changing the beam density also affects the plasma density. Therefore the above-mentioned measurement was not the result of a simple parameter change. Further investigations are necessary to discover the true density-frequency dependence.

Theoretical Model of the Beam

The beam used in our experiment is a cylindrical shell of thickness τ and radius r (see Fig. XXIII-10). It has zero-order azimuthal and axial velocity components. This zero-order motion is established by the magnetic field so that the azimuthal velocity is

$$v_\perp = r\omega_{ce}.$$

The beam is assumed to be neutralized by infinitely massive ions. The effects of slip are ignored.

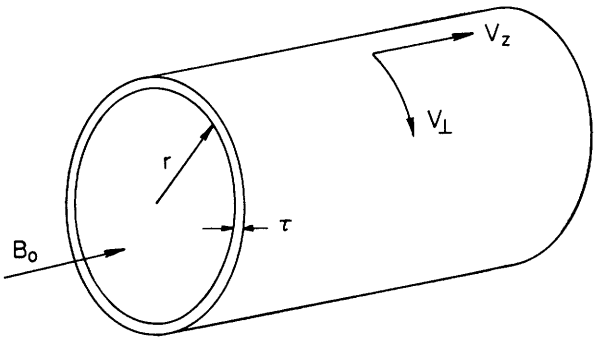

Fig. XXIII-10. Cylindrical beam.

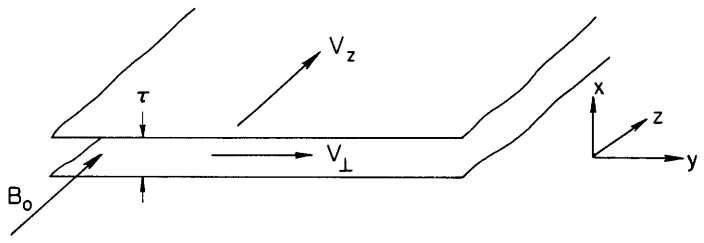

Fig. XXIII-11. Sheet beam.

To model this beam we have unwrapped it to form a sheet beam as shown in Fig. XXIII-11. We require that the wavelength in the y direction fit around the circumference of the cylindrical beam an integral number of times. The first-order variations on this sheet beam then go as

$$e^{j\left(\omega t - \frac{m}{r} y - kz\right)}, \qquad m = 0,\ 1,\ 2 \ldots .$$

We assume a first-order perturbation of the beam particles given by

$$\bar{\delta} = \bar{i}_x \delta_x(y, z, t) + \bar{i}_y \delta_y(y, z, t) + \bar{i}_z(y, z, t),$$

and that the beam density varies as a Gaussian function of x. Performing a rigid beam analysis[2] gives a set of homogeneous equations for the components of δ

$$\begin{aligned}
\Omega^2 \delta_x &= \omega_1^2 \delta_x - j\Omega\omega_{ce}\delta_y \\
\Omega^2 \delta_y &= \omega_2^2 \delta_y + \omega_3^2 \delta_z + j\Omega\omega_{ce}\delta_x \\
\Omega^2 \delta_z &= \omega_4^2 \delta_y + \omega_5^2 \delta_z,
\end{aligned} \tag{1}$$

where $\Omega = \omega - m\omega_{ce} - kv_{ce}$ and the ω_ℓ^2 are reduced beam-plasma frequencies.

$$\omega_\ell^2 = \omega_{pb}^2 R_\ell, \qquad (\ell = 1, 2, 3, 4, 5), \qquad R_\ell < 1.$$

Here, ω_{pb} is the beam-plasma frequency at the center of the beam, and

$$R_1 = \frac{1}{\sqrt{2\pi}} - \frac{\sqrt{\frac{m^2}{r^2} + k^2}\,\tau}{2\sqrt{\pi}} Z_i\left(j\frac{\sqrt{\frac{m^2}{r^2} + k^2}\,\tau}{\sqrt{2}}\right)$$

$$R_2 = \frac{m^2 \tau}{2\sqrt{\pi}\, r^2 \sqrt{\frac{m^2}{r^2} + k^2}} Z_i\left(j\frac{\sqrt{\frac{m^2}{r^2} + k^2}\,\tau}{\sqrt{2}}\right)$$

$$R_3 = \frac{kr}{m} R_2$$

$$R_4 = R_3$$

$$R_5 = \frac{k^2 r^2}{m^2} R_2,$$

with Z_i the imaginary part of the plasma dispersion function.

The dispersion relation follows directly from Eqs. 1 and can be placed in the form

$$0 = \Omega^4 - \Omega^2\left(\omega_1^2+\omega_2^2+\omega_5^2+\omega_{ce}^2\right) + \omega_1^2\omega_5^2 + \omega_2^2\omega_1^2 + \omega_5^2\omega_2^2 - \omega_3^4. \tag{2}$$

This dispersion relation was investigated for three values of m; 0, 1, and 2. Real values were chosen for k and the four values of ω were obtained. The results are shown in Figs. XXIII-12 through XXIII-15.

The dispersion relation for m = 0 is degenerate because $\omega_2^2 = \omega_3^2 = \omega_4^2 = 0$, and the relation becomes

$$\left(\Omega^2-\omega_{ce}^2-\omega_1^2\right)\left(\Omega^2-\omega_5^2\right) = 0. \tag{3}$$

The equations for the components of δ also uncouple.

$$\begin{aligned}
\Omega^2\delta_x &= \omega_1^2\delta_x - j\Omega\omega_{ce}\delta_y \\
\Omega^2\delta_y &= j\Omega\omega_{ce}\delta_x \\
\Omega^2\delta_z &= \omega_5^2\delta_z.
\end{aligned} \tag{4}$$

It can be seen that the waves $\Omega^2 - \omega_5^2 = 0$ are made up of particle motion only in the z-direction, with the particles oscillating at a reduced plasma frequency ω_5. There is no dependence on the magnetic field. The particle motion is characteristics of a longitudinal wave. The second set of waves, $\Omega^2 - \omega_{ce}^2 - \omega_1^2 = 0$, is made up of particle motion across the magnetic field. The polarization of this motion is circular for small wavelength, becoming elliptical for longer wavelengths. One of these waves has a phase velocity less than the beam velocity and is right polarized. The other wave has a plasma velocity greater than the beam velocity and is left polarized. These are therefore very similar to cyclotron waves.

These m = 0 beam waves are shown in Fig. XXIII-12 for the condition $\omega_{ce} > \omega_{pb}$. The positive and negative energy waves are labeled (+) and (-), respectively. Figure XXIII-13 shows the m = 0 waves for the condition $\omega_5 > \omega_{ce}$. Although the cyclotron and longitudinal waves intersect, they do not couple.

The beam waves for m = 1, and with $\omega_{ce} > \omega_{pb}$ are shown in Fig. XXIII-14. For these waves, the x, y, and z particle motions all couple; however, the waves still have properties similar to the m = 0 waves previously described. The waves labeled A and B are essentially cyclotron waves. For small wavelengths their transverse motion is circularly polarized with negligible z-displacement. As the wavelength increases the transverse motion becomes slightly elliptical and the z component increases. The

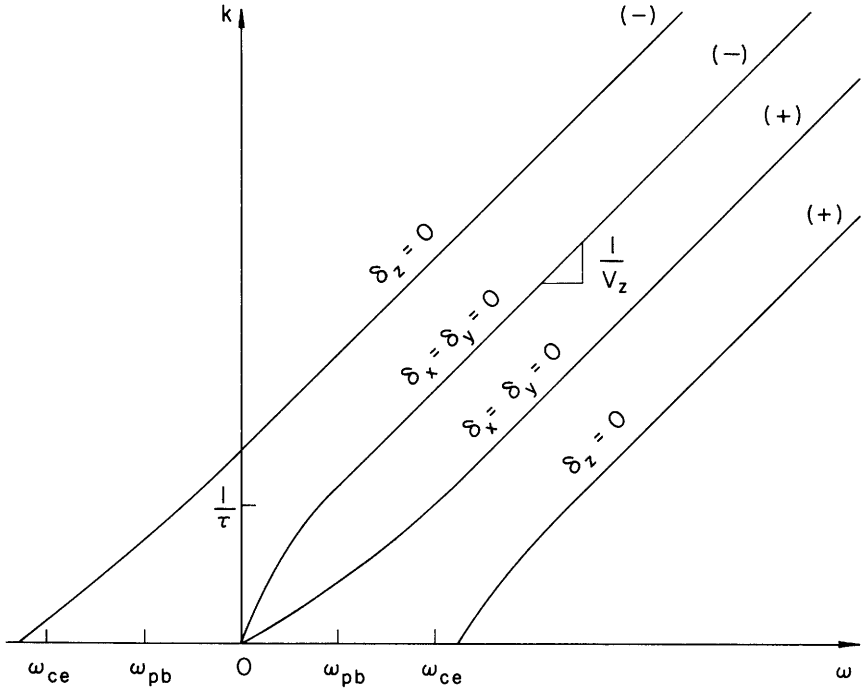

Fig. XXIII-12. Beam waves; m = 0, $\omega_{ce} > \omega_{pb}$.

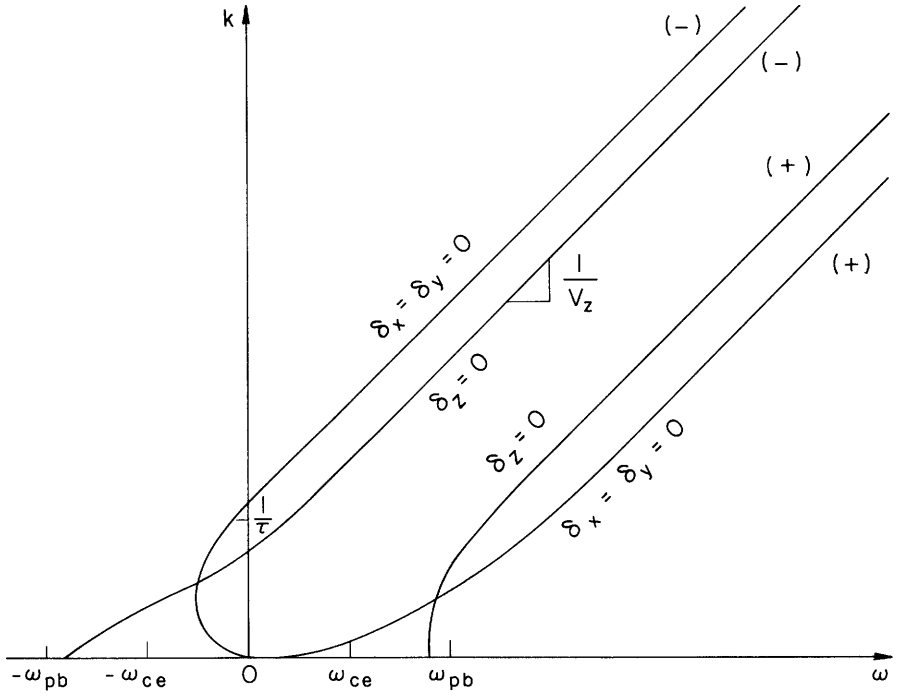

Fig. XXIII-13. Beam waves; m = 0, $\omega_5 > \omega_{ce}$.

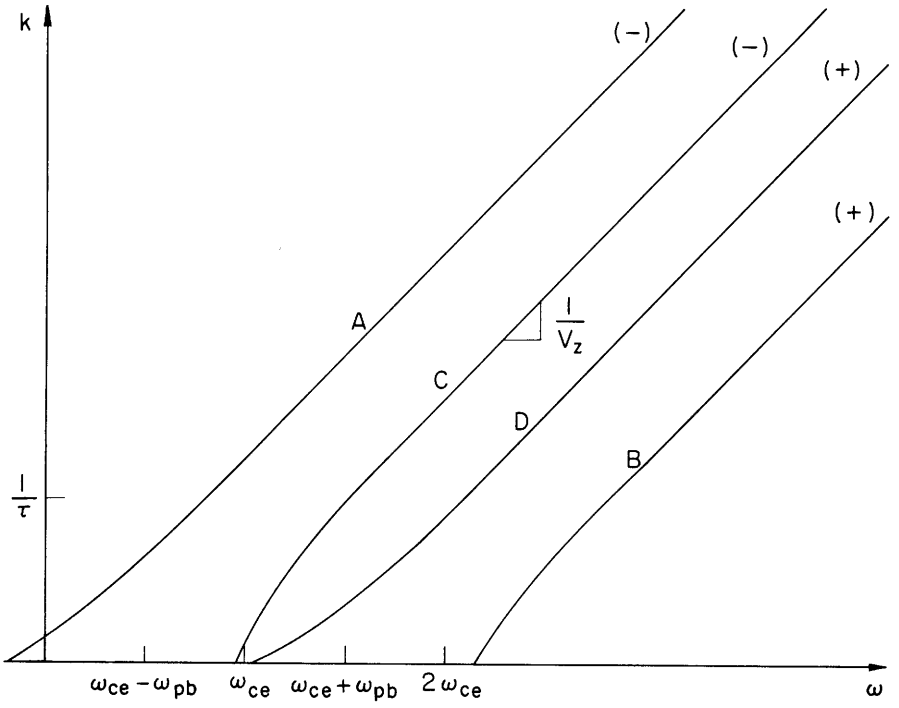

Fig. XXIII-14. Beam waves; m = 1, $\omega_{ce} > \omega_{pb}$.

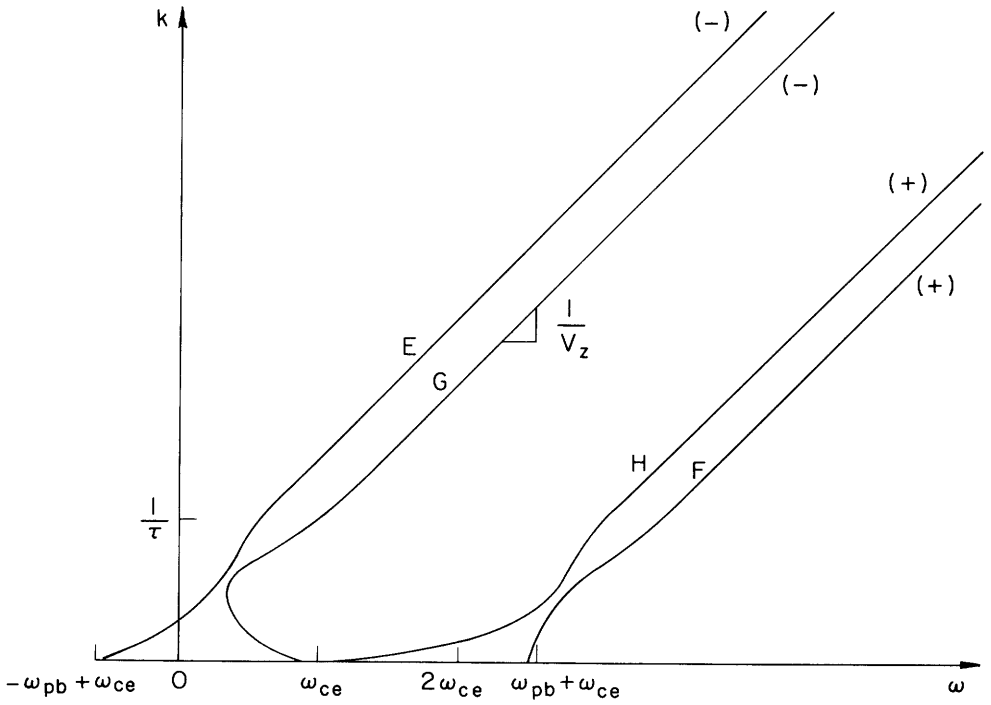

Fig. XXIII-15. Beam waves; m = 1, $\omega_5 > \omega_{ce}$.

waves labeled C and D are similar to longitudinal waves. Particle motion for small wavelength is z-directed, for the most part, with negligible transverse components. As the wavelength increases the transverse motion increases.

The dispersion for m = 1, $\omega_5 > \omega_{ce}$ is shown in Fig. XXIII-15. Here the roots couple. The solutions E and F, for short wavelength, behave like longitudinal waves. As the wavelength increases above the beam thickness these solutions become similar to waves A and B of Fig. XXIII-14. The solutions G and H are similar to cyclotron waves for short wavelength. For long wavelengths these solutions have the characteristics of waves C and D of Fig. XXIII-14.

The waves for m = 2 and higher modes are similar to the m = 1 waves, except that the Doppler shift is $m\omega_{ce}$.

We are now in the process of investigating the coupling of these beam waves with waves of a plasma background.

B. R. Kusse, A. Bers

References

1. B. Kusse, A. Bers, "Interaction of a Spiraling Electron Beam with a Plasma," Quarterly Progress Report No. 86, Research Laboratory of Electronics, M.I.T., July 15, 1967, pp. 154-156.

2. B. Kusse, "Interactions of a Spiraling Electron Beam with a Plasma," Quarterly Progress Report No. 87, Research Laboratory of Electronics, M.I.T., October 15, 1967, pp. 115-120.

3. BEAM SPACE-CHARGE-WAVE INTERACTION WITH THE BACKWARD WAVE IN A COLD-PLASMA WAVEGUIDE

We have begun a systematic investigation of high-frequency beam-plasma interactions in a plasma-filled waveguide. One interaction that has not been studied in detail in the past is the beam space-charge-wave interaction with the backward plasma wave near ω_{pe}, for the case $\omega_{pe} > \omega_{ce}$. We present here some results of a recent study of this interaction, in which collisional effects were included.

The model considered is that of an electron beam traveling with velocity v_o through a cold electron plasma uniformly filling a circular waveguide, with a uniform axial magnetostatic field B_o imposed on the system. Neglecting ion motion and assuming quasi-static waves of the form $\exp(j\omega t - jk_z z)$, where k_z is the wave number along the axis of the waveguide, we find that the dispersion equation for the space-charge-wave (or m = 0) interaction is

$$(\omega - k_z v_o)^2 \left[k_z^2 K_{\parallel}(\omega) + p^2 K_{\perp}(\omega) \right] = k_z^2 \omega_b^2, \tag{1}$$

where

p = transverse wave number in the waveguide

ω_b = "effective" beam-plasma frequency, which depends on the beam density profile[1]

$$K_{\parallel}(\omega) = 1 - \frac{\omega_{pe}^2}{\omega^2 (1 - j\nu_c/\omega)} \tag{2}$$

$$K_{\perp}(\omega) = 1 - \frac{\omega_{pe}^2 (1 - j\nu_c/\omega)}{\omega^2 (1 - j\nu_c/\omega)^2 - \omega_{ce}^2} \tag{3}$$

ν_c = collision frequency for plasma electrons.

By analogy with the backward-wave oscillator, it has been argued[2] that an absolute instability should arise when the slow beam space-charge-wave interacts with the backward-propagating plasma wave just above ω_{pe} ($\omega_{pe} > \omega_{ce}$). By applying the Bers-Briggs instability criteria[2] to the dispersion equation (1), we found that this absolute instability did exist in the limit of zero collision frequency and a very weak beam. We also found, however, the following facts regarding this "backward-wave" interaction:

(i) As the effective beam-plasma frequency ω_b is increased from zero, in the absence of collisions, there is a transition (at some critical ω_b) from an absolute

instability near ω_{pe} to "infinite spatial amplification" at ω_{pe}. As ω_b is further increased the absolute instability is eliminated. This critical value of ω_b (for $\nu_c = 0$) is a function of the plasma parameters. When $(pv_o)^2 \ll \omega_{pe}^2 - \omega_{ce}^2$, this critical value of ω_b at the transition is given by

$$\frac{\omega_b}{\omega_{pe}} = \frac{\left(\frac{pv_o}{\omega_{pe}}\right)\left(\frac{\omega_{ce}}{\omega_{pe}}\right)}{\sqrt{1-\left(\frac{\omega_{ce}}{\omega_{pe}}\right)^2}}. \tag{4}$$

This expression vanishes as $p \to 0$, thereby showing that there is no region of absolute instability for the one-dimensional case, as is well known.

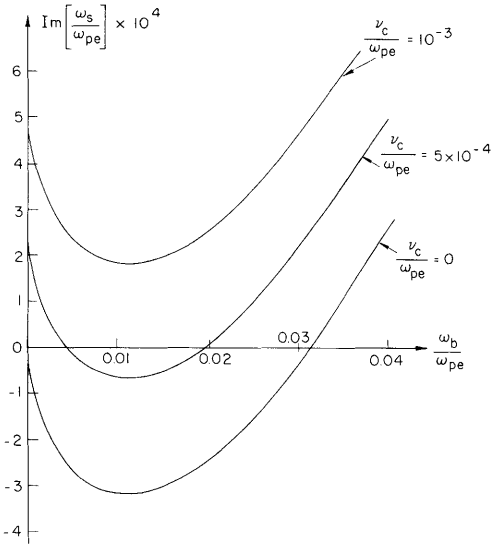

Fig. XXIII-16.

Imaginary part of branch pole frequency ω_s as a function of ω_b, with collision frequency ν_c as parameter. (Note: Re $(\omega_s/\omega_{pe}) \approx 1$). Plasma parameters: $pv_o/\omega_{pe} = 0.054$; $\omega_{ce}/\omega_{pe} = 0.5$.

(ii) As the collision frequency ν_c is increased from zero with ω_b fixed, the absolute instability (if it originally existed) becomes weaker and is ultimately replaced by a convective instability with a finite spatial growth rate. In case an infinite amplification is observed in the absence of collisions, a finite spatial amplification is obtained when collisions are included.

These statements may be clarified by the accompanying diagrams. Figure XXIII-16 shows the imaginary part of the branch pole frequency ω_s as a function of ω_b, with collision frequency ν_c as a parameter. (Corresponding to the branch pole ω_s, there is a saddle point $k_z(\omega_s)$ in the complex k_z-plane, formed by the merger of two roots coming from opposite halves of the k_z-plane as Im (ω) is increased from $-\infty$.) An absolute instability is indicated when Im $(\omega_s) < 0$. It is seen that increasing ω_b or ν_c, or both, will bring the branch pole into the upper-half ω-plane, with the result that there is a

transition from absolute to convective instability.

In the region of convective instability, the solid curves in Fig. XXIII-17 give the maximum spatial amplification rate (near $\omega = \omega_{pe}$) as a function of collision frequency ν_c, with ω_b as parameter. For comparison, the broken curves in Fig. XXIII-17 give the

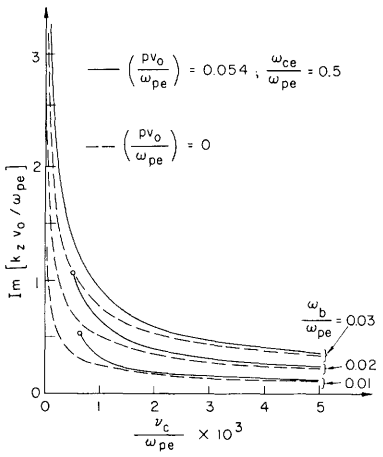

Fig. XXIII-17.

Maximum spatial amplification rate (at $\omega \approx \omega_{pe}$) as a function of collision frequency ν_c, with ω_b as parameter. Solid curves are for a waveguide of finite radius ($p \neq 0$); broken curves are for a waveguide of infinite radius and wave propagation along the magnetostatic field ($p = 0$). Small circles terminate the solid curves at points of transition from convective to absolute instability.

maximum amplification rate (again near ω_{pe}) for the one-dimensional case ($p = 0$). It was found that in the presence of collisions the one-dimensional model gave fairly good values for the maximum amplification rate when $\frac{pv_o}{\omega_{pe}} \ll 1$, $\left(\frac{\omega_{ce}}{\omega_{pe}}\right)^2 \ll 1$, and ω_b was properly adjusted to account for the finite size of the beam.

S-L. Chou, A. Bers

References

1. S. Chou and A. Bers, "Thin Electron-Beam Interactions with Ions in a Plasma-filled Waveguide," Quarterly Progress Report No. 87, Research Laboratory of Electronics, M.I.T., October 15, 1967, pp. 89-99.
2. R. J. Briggs, Electron-Stream Interaction with Plasmas (The M.I.T. Press, Cambridge, Mass., 1964).

4. CRITICAL LENGTHS FOR ABSOLUTE INSTABILITIES

The classification of unstable modes in infinite uniform systems as either absolute or convective can be of considerable intuitive benefit when reasoning about the stability of an actual finite and inhomogeneous system. For a convective instability, the amplification rate (Im k for real ω) provides a measure of the system lengths for which the unstable mode is important. (Precise statements require a careful consideration of wave reflection at the ends; the important point to be stressed here is that at least the general order of magnitude of the critical system lengths can be inferred from the uniform system theory.) A uniform system that supports an absolute instability, on the other hand, has a "built-in" feedback mechanism. It is well-known that there are usually minimum system lengths for absolute instabilities to occur, these critical lengths relating essentially to the strength of the internal feedback mechanisms. The purpose of this report is to indicate a possible method for identifying the critical lengths associated with absolute instabilities.[1]

Construction of Eigenmodes in the WKB Approximation

We consider a slowly varying medium with parameters such that the local dispersion relation predicts absolute instability over the region $-\frac{L}{2} < z < \frac{L}{2}$ (see Fig. XXIII-18).

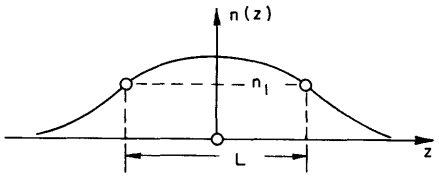

Fig. XXIII-18. Inhomogeneous medium in which a parameter (for example, the plasma density $n<z$) varies smoothly. The local dispersion relation predicts absolute instability over the region L where $n > n_1$.

For a slowly varying medium, one is led to consider solutions for the physical variable ψ of the WKB form:

$$\psi(z,\omega) \sim \exp\left(-j\int^{z} k_n(\omega,z)\,dz\right), \tag{1}$$

where $k_n(\omega,z)$ is one of the solutions to the local dispersion equation, and ω is the usual Laplace transform variable. If one imagines a localized source situated in the central region (for example, $\delta(z)\,\delta(t)$), then it might appear at first sight that the solutions on either side of the source would contain a sum of terms of the form of Eq. 1, where the $k_n(\omega,z)$ appropriate to either side are selected by the same "rules of causality" as in the infinite uniform system. The WKB solution is valid, however, only in regions where

$$\frac{\frac{dk}{dz}}{k^2} < 1. \tag{2}$$

In a system that exhibits absolute instability, there is a "degeneracy" ($k_1 = k_2$) of positive (k_1)-going and negative (k_2)-going waves at a critical (saddle-point) frequency ω_s. In a nonuniform system, this saddle-point frequency is a function of position, and near $\omega_s(z)$, therefore,

$$k_{1,2} \approx k_o \pm \alpha\sqrt{\omega_s(z) - \omega}, \tag{3}$$

and $\frac{dk}{dz} \to \infty$ at any position z_o, where $\omega_s(z_o) = \omega$. This means, as we shall describe in more detail, that in the case of a nonuniform system the presence of a "pinch" like that associated with an absolute instability leads to a "reflection" of the wave in the vicinity of the (possibly complex) position z_o. Since there would be a complementary reflection point at $-z_o$ in a symmetrical system, we are led to the tentative conclusion that there is a close connection between the existence of "confined" unstable eigenmode solutions to the inhomogeneous media problem, on the one hand, and the prediction of absolute instability from the local dispersion relation. Furthermore, the eigenfrequencies associated with such a finite-system eigenmode approach the uniform-system saddle points as $L \to \infty$.

We now wish to demonstrate the correctness of these assertions. We shall <u>assume</u> that the response can be developed, using only the two wave numbers that are involved in the absolute instability pinch. (This assumption should be valid at least in the limit of very large L; we cannot offer any concrete conditions for its validity otherwise, except to note that if another root (k_3 say) undergoes a "metamorphosis" with k_1 or k_2 in the region of interest, it should also be included in the expression for $\psi(\omega, z)$.) With this assumption, we write

$$\psi(z,\omega) = Ag_1(z) \exp - j \int^z k_1(\omega, z)\, dz$$

$$+ Bg_2(z) \exp - j \int^z k_2(\omega, z)\, dz, \tag{4}$$

where g_1 and g_2 are slowly varying relative to the exponentials when the WKB solutions are valid. Let

$$q(\omega, z) = \frac{1}{2}(k_1(\omega, z) - k_2(\omega, z)) \tag{5}$$

and $z_a(\omega)$, $z_b(\omega)$ be the positions where $k_1 = k_2 (q = 0)$. For a general N-wave system, one can show from the coupled first-order equations that for the WKB solutions in Eq. 4

$$g_1(z) \sim g_2(z) \sim 1/\sqrt{q} \tag{6}$$

in the vicinity of the points where $q = 0$.[3] (One can also readily demonstrate Eq. 6 for

electrostatic plasma waves, since in that case $g = \left(\frac{\partial \epsilon}{\partial k}\right)^{-1/2}$, where $\epsilon(\omega, k, z)$ is the dielectric constant, and $\epsilon = 0$ is the local dispersion relation.[2] Near a double root of the dispersion relation at k_s, therefore $\left(\frac{\partial \epsilon}{\partial k}\right)_{k_1} \sim k_1 - k_s \sim q$, etc.)

This result suggests that we write Eq. 4 in the form

$$\psi(z,\omega) = \left[Ag_1(z)\exp\left(-j\int_{z_a}^{z} q(\omega,z)\,dz\right) + Bg_2(z)\exp\left(+j\int_{z_a}^{z} q(\omega,z)\,dz\right)\right] \cdot \exp\left[-j\int^{z}\left(\frac{k_1+k_2}{2}\right)dz\right]. \tag{7}$$

The fact that the exponential factor $\frac{1}{2}(k_1+k_2)$ is well-behaved at z_a and z_b, and also that g_1 and g_2 behave as in Eq. 6 near $q = 0$, means that our problem is essentially identical in form to the classical WKB solution of the second-order inhomogeneous wave equation. (See, for example, Heading.[4]) In Fig. XXIII-19a, we have sketched the general form that the Stokes and anti-Stokes lines emanating from the critical point z_a must have for an eigenmode to be constructed. In the section bounded by A_1 and A_2, which includes the positive real z axis by assumption, the solution must involve only outgoing waves, (the term with $k_1(\omega, z)$) so $B = 0$ in this domain. Furthermore, since by assumption the plasma becomes stable for $z \to +\infty$, the locus of the roots of $k(\omega, z)$ as $z \to \infty$ must be as shown in Fig. XXIII-19b for any ω in the lower half-plane. Therefore, the solution for $z \to \infty$ contains only the subdominant term in the general WKB solution (Eq. 7), and by the general rules for tracing the asymptotic solutions round the critical points, we find that $B = jA$ in the domain bounded by S_2 and S_3. We can apply dual arguments to the metamorphosis of the solution around the other turning point (z_b), which must involve only the outgoing wave (k_2) for $z \to -\infty$. The consistency of these solutions imposes the usual quantization condition

$$\int_{z_b(\omega)}^{z_a(\omega)} q(\omega,z)\,dz = \left(n+\frac{1}{2}\right)\pi. \tag{8}$$

We stress again that the formulation of this determinantal equation for the eigenfrequencies is based on the assumption that the Stokes and anti-Stokes lines of $q(\omega, z)$ are as shown in Fig. XXIII-19, and also on the assumption that the medium is stable for $z \to \pm\infty$ so that the appropriate solutions in these regions, as dictated by causality, are also the subdominant terms in Eq. 7.

We shall use Eq. 8 below to examine a simple case of absolute instability that has aplication to the microwave tube field. In order to illustrate the qualitative features of the eigenfrequencies predicted by Eq. 8, we shall now consider a case in which the system parameters are roughly constant over some region L,

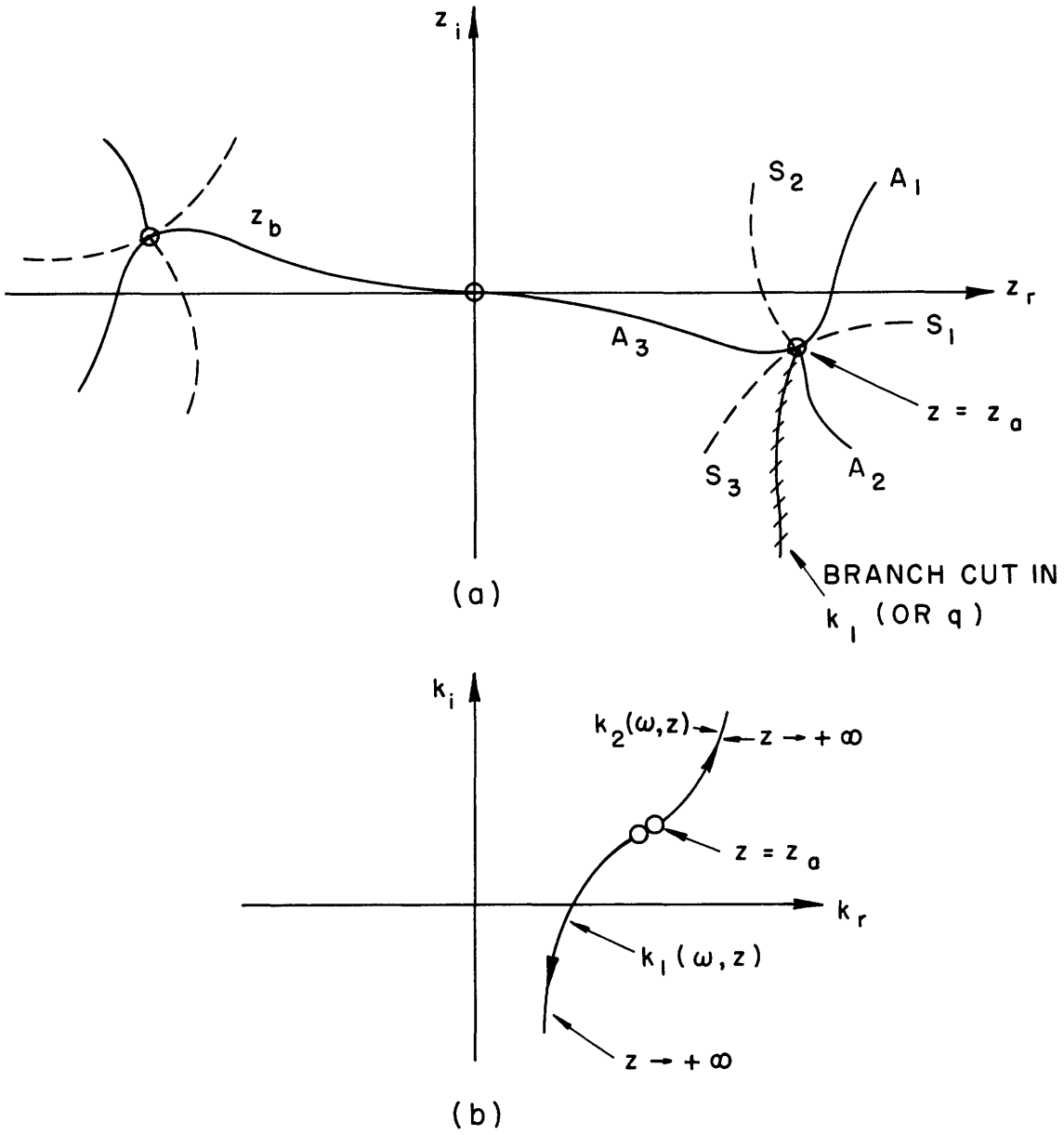

Fig. XXIII-19. (a) Stokes and anti-Stokes lines in the complex z-plane.
(b) Motion of wave numbers away from pinch as z varies.

$z_a(\omega)$ and $z_b(\omega)$ are the points where $q(\omega, z) = 0$.

A_1, A_2, A_3 are the anti-Stokes lines.

S_1, S_2, S_3 are the Stokes lines.

so that we can approximate Eq. 8 by

$$qL = \frac{1}{2}(k_1(\omega)-k_2(\omega))\ L \approx \left(n+\frac{1}{2}\right) \tag{9}$$

where k_1 and k_2 are now considered independent of z. This approximation should be valid at least in the limit of large L, where the eigenfrequencies approach the infinite-system frequency (ω_s) as $L \to \infty$. For $L < \infty$, Eq. 9 suggests that we obtain the finite-system eigenfrequencies by solving for the ω values that satisfy

$$\text{Im}\ (k_1(\omega)-k_2(\omega)) = 0$$

$$\text{Re}\ (k_1(\omega)-k_2(\omega)) = \pi/L. \tag{10}$$

A schematic illustration of the solution of Eq. 10 is shown in Fig. XXIII-20, and shows how the frequencies depart from the infinite system values as L is decreased. If the absolute instability is weak enough so that the departure of k_1 and k_2 from k_s is not too great, this procedure can in some cases give us the actual critical length where Im (ω) passes through zero.

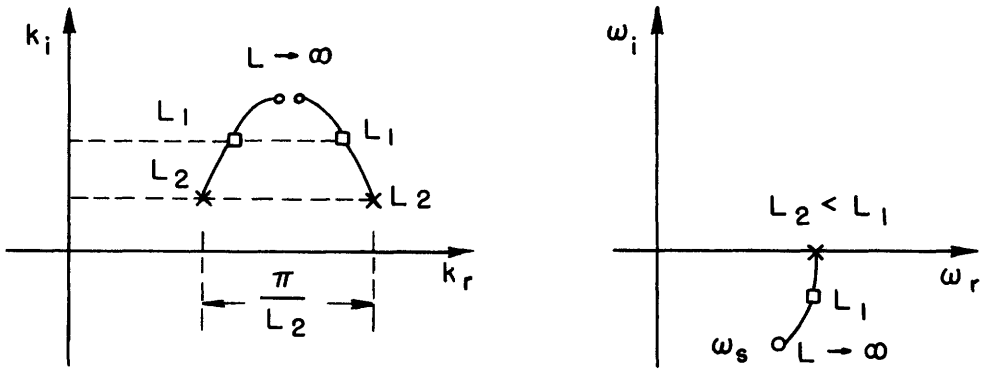

Fig. XXIII-20. Solution for the eigenfrequencies as a function of L, with Eq. 10 used.

Also note that the departure of ω from ω_s in the limit of large L can be explicitly derived from the expansion

$$\omega - \omega_s \approx \frac{1}{2}\left(\frac{\partial^2\omega}{\partial k^2}\right)_s (k-k_s)^2$$

$$\approx \frac{1}{2}\left(\frac{\partial^2\omega}{\partial k^2}\right)\left(\frac{\pi}{2L}\right)^2 \tag{11}$$

Example of Coupled Modes

The weak coupling of two propagating modes, when one wave is a negative energy mode and the other is a backward wave, is a classic example of an absolute

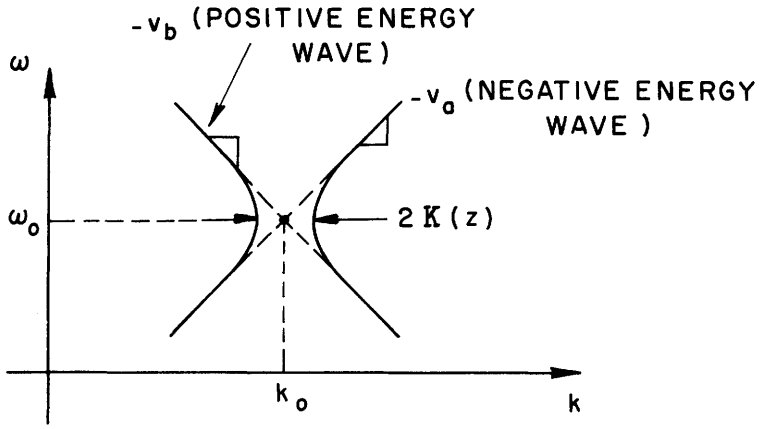

Fig. XXIII-21. Local dispersion of the coupled-mode example in the (ω-K)-plane.

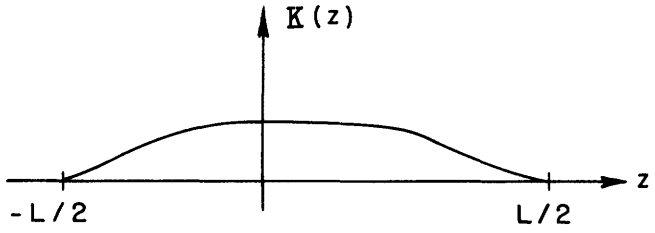

Fig. XXIII-22. Form of coupling constant as a function of z.

instability (see Fig. XXIII-21). If we model the finite system as a gradually varying spatial coupling constant K(z) that goes to zero outside the region $-\frac{L}{2} < z < \frac{L}{2}$ (Fig. XXIII-22), then the local dispersion relation becomes

$$\left(\tilde{k}-\frac{\tilde{\omega}}{v_a}\right)\left(k+\frac{\tilde{\omega}}{v_b}\right) = K^2(z), \tag{12}$$

where $\tilde{k} = k - k_o$ and $\tilde{\omega} = \omega - \omega_o$. For this case,

$$q(\omega, z) \equiv \frac{1}{2}(k_1 - k_2)$$

$$= \left(\frac{\omega^2}{v_s^2} + K^2(z)\right)^{1/2} \tag{13}$$

with $1/v_s \equiv \frac{1}{2}(1/v_a + 1/v_b)$. As an example, consider the parabolic form

$$K^2(z) = K_o^2\left[1 - \left(\frac{2z}{L}\right)^2\right]. \tag{14}$$

An elementary calculation from Eq. 8 gives the eigenfrequencies

$$\frac{\tilde{\omega}^2}{v_s^2} = (2n+1)\frac{2K_o}{L} - K_o^2, \tag{15}$$

and the critical length

$$L_{crit} = \frac{2}{K_o}. \tag{16}$$

In terms of the average coupling constant, $\langle K\rangle = \frac{\pi}{4}K_o$, the critical length is

$$L_{crit} = \frac{\pi}{2}\frac{1}{\langle K\rangle}. \tag{17}$$

Equation 17 is a general result, as can be seen from Eq. 13, since $\omega = 0$ at the onset of the finite-system instability.

This critical length is in precise agreement with the boundary-value solution of the uniform-coupling problem,[5] except for the fact that the coupling constant is averaged in the WKB case. The important general lesson to be learned from this example is the fact that the system length for instability is related to the "beat wavelength" ($\sim(k_1-k_2)^{-1}$), and not to the total wavelength ($\sim\pi/k_o$). In physical applications of the present example, these two wavelengths can differ by orders of magnitude.

R. J. Briggs

References

1. A somewhat similar approach has recently been described by M. N. Rosenbluth, H. Berk, and D. Pearlstein, 9th Annual Meeting of the Division of Plasma Physics, American Physical Society, Austin, Texas, November 8-11, 1967.
2. H. L. Berk, M. N. Rosenbluth, and R. N. Sudan, Phys. Fluids 9, 1606-1608 (1966).
3. C. Budden, Radio Waves In the Ionosphere (Cambridge University Press, London, 1961).
4. G. Heading, An Introduction to Phase Integral Methods (Methuen, London; John Wiley and Sons, Inc., New York, 1962).
5. See, for example, W. H. Louisell, Coupled Mode and Parametric Electronics (John Wiley and Sons, Inc., New York 1960).

XXIII. PLASMAS AND CONTROLLED NUCLEAR FUSION*

B. Applied Plasma Physics Related to Controlled Nuclear Fusion

Academic and Research Staff

Prof. T. H. Dupree
Prof. L. M. Lidsky
Prof. N. L. Oleson
Prof. S. Yip
Dr. R. A. Blanken

Graduate Students

T. S. Brown
K. R-S. Chen
D. G. Colombant
C. T. Dum
R. W. Flynn
M. Hudis
G. R. Odette
D. H. Ross
A. Sugawara
C. E. Wagner

RESEARCH OBJECTIVES

1. Radiation Damage Studies

Radiation damage by 14.2-MeV D-T fusion neutrons will be an important consideration for any controlled fusion reactor. We have built and operated a sensitive internal-friction spectrometer to measure damage caused by small doses of 14.2-MeV neutrons and have developed a theoretical model to allow us to estimate the extent of 14.2-MeV neutron damage by extrapolation from lower energy radiation data (fission spectra, for example). These extrapolation techniques will be tested by applying them to comparison of samples irradiated in the M. I. T. reactor and in the Department of Nuclear Engineering's Cockcraft-Walton neutron generator.

G. R. Odette

2. Experimental Instability and Diffusion Studies

The long "quiescent" plasma column developed here by J. C. Woo is being used by several investigators. "On-line" correlation techniques have been developed to investigate the spectrum of oscillations that are present in the column and, in particular, we have identified and are studying several species of drift wave. We hope to pin down the drift-wave driving terms and to measure saturated wave amplitudes to test certain predictions of nonlinear plasma kinetic theory. We are also investigating the average particle lifetime in the plasma for a wide variety of conditions and have just begun an experiment aimed at the direct measurement of local values of the diffusion current.

D. H. Ross, M. Hudis, R. A. Blanken,
L. M. Lidsky, N. L. Oleson

3. Intense Neutron Sources

Preliminary calculations indicate that it may be possible to build a 14-MeV neutron source with 10^{15} n/cm^2 sec intensity at the target position by using the Mach cone of a freely expanding jet as a windowless gas target. A detailed investigation of such neutron sources has been started, with the primary objective of solving the hydrodynamic equations for duct flow with intense heating. This will be followed by an analysis of the system to find the optimal pressure ratios, expansion factors, diffusor design, and so forth.

D. G. Colombant, L. M. Lidsky

*This work was supported by the National Science Foundation (Grant GK-1165).

4. Confinement of Hot-Electron Plasmas

We have generated beam-plasma discharge plasmas in mirror, cusp, and stuffed-cusp magnetic fields and are engaged in measurements of their similarities and differences. The mirror-contained plasma is distinguished from the cusp-contained plasma, for example, by a much higher temperature for the energetic group (35 keV versus ~10 keV) and a higher level of density fluctuation. We plan to identify the types of instabilities which are present in these several systems, giving special attention to distinguishing the instabilities driven by the high- and low-energy electron groups.

C. E. Wagner, L. M. Lidsky

5. Particle Motion in Large-Amplitude Waves

We are attempting to calculate the time evolution of the distribution function for a single nonlinear wave. We hope that the solution of this problem can then be applied to strong narrow-band turbulence. In this regime, particle trapping, or strong reflections from potential maxima, is an important feature of the motion. This feature is not included in present weak-turbulence theory.

T. S. Brown, T. H. Dupree

6. Computer Experiments on Turbulent Plasma

A computer program has been written to compute the particle distribution function for a given arbitrary spectral density of the electric field. The influence of the spectrum on particle motion can be studied in detail and compared with various theories. The distribution function and the electric field are not required to satisfy Maxwell's equation. Dropping this "self-consistency" constraint leads to a much more accurate computer simulation of the Vlasov equation, and also gives the experimeter complete freedom to specify the spectrum.

R. W. Flynn, T. H. Dupree

7. Nonlinear Wave-Particle Interaction in a Turbulent Plasma

As a result of wave-particle interactions, particle trajectories deviate from the unperturbed orbits used in standard perturbation theory. This gives higher order secular terms when solving the Vlasov-Maxwell equations. A new perturbation theory is being studied in which a statistical set of perturbed orbits is used, so that it leads principally to a broadening of wave-particle resonances.

Wave-particle interactions in the presence of a static magnetic field are being investigated by using this method. The results will be used to assess the importance of nonlinear effects on growth rates and diffusion coefficients for some major types of instabilities.

C. T. Dum, T. H. Dupree

1. PARTICLE FLUX MEASUREMENTS IN A HOLLOW-CATHODE ARC

Recent alkali-plasma experiments have shown that low frequency oscillations either are[1] intimately connected with enhanced plasma diffusion or they are not.[2] Chu, Handel and Politzer show that local values of the diffusion coefficients inferred from values of $\langle \Delta n \cdot \Delta \phi \rangle$ agree with global estimates of total plasma loss rates. In their experiments the density and potential fluctuations were caused by collisional drift waves. In a very

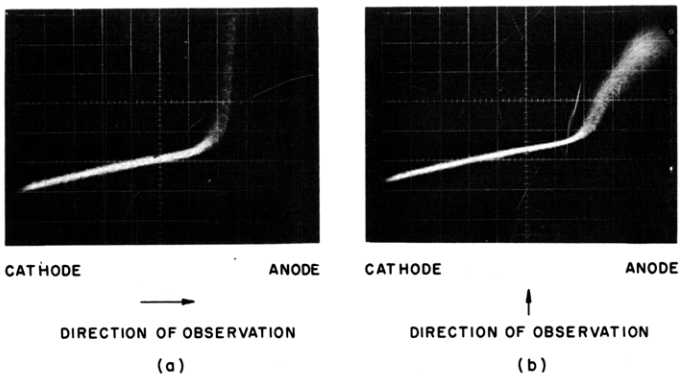

Fig. XXIII-23. Probe curves from measurements with a one-sided flat Langmuir probe. Vertical axis: probe current, -5 mA/cm. Horizontal axis: probe voltage, 13.8 V/cm.

(a) Ion saturation current, 2.5 mA; $T_e = 3.28$.

(b) Ion saturation current, 1 mA; $T_e = 4.2$.

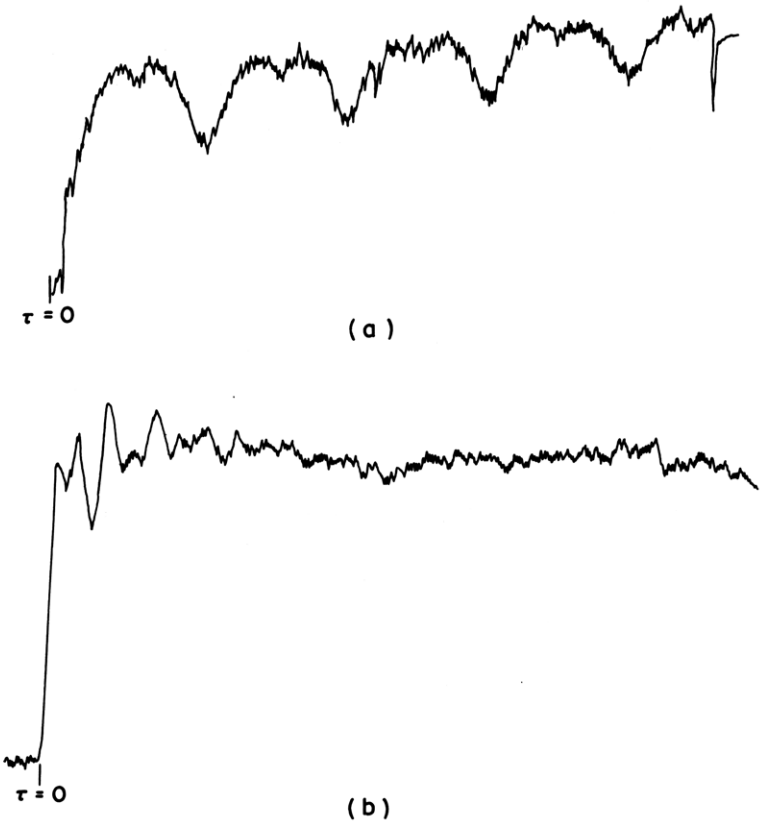

Fig. XXIII-24. Autocorrelation of signals for two probe directions.

(a) Horizontal axis: time delay, 12.7 μsec/cm.
(b) Horizontal axis: time delay, 2.6 μsec/cm.

similar measurement performed by F. Chen, it has been that the fluctuations in density and potential were almost exactly in quadrature, and that the particle losses could not be attributed to drift-wave driven processes. We plan to measure the enhanced particle flux directly, and thus to shed light on the mechanisms of instability-driven diffusion.

The net radial flux in the plasma column is approximately 40 db below the random (Nv/4) current and, we guess, ~20 db below low-frequency random fluctuations in the current for the most quiescent possible state of the plasma.[3] To assess the feasibility of dredging this signal from the noise, we have been measuring the axial and azimuthal drift currents, which are ~20 db greater than the radial currents of interest. Experience has shown that gains in excess of 20 db in S/N ratios are possible with synchronous detection techniques.

These preliminary measurements pointed up an unsuspected feature of the plasma column – it is very highly anisotropic. Figure XXIII-23 shows probe curves measured with a one-sided flat Langmuir probe. If these curves are interpreted by simple probe theory, Fig. XXIII-23a indicates an electron temperature of 3.3 eV and total ion density 6×10^{12} cm^{-3}; Fig. XXIII-23b, made with the probe facing in the direction of azimuthal E/B rotation, indicates an electron temperature of 4.2 eV and azimuthal velocity of 10^5 cm/sec. The asymmetry is apparent also in autocorrelation traces of potential fluctuations. Figure XXIII-24 shows autocorrelation of the signals obtained for two different probe directions.

The ease with which azimuthal fluxes are measured augurs well for the attempt to measure radial flux; we shall construct a two-sided rotating probe for these measurements. For rotational frequency ω, the diffusion flux will constitute a current modulation at frequency $\omega/2$.

M. Hudis, L. M. Lidsky

References

1. T. K. Chu, H. W. Handel, and P. A. Politzer, "Measurements of Enhanced Plasma Losses by Collisional Drift Waves," Phys. Rev. Letters 19, 1110 (November 6, 1967).
2. J. Woo, Quarterly Progress Report No. 76, Research Laboratory of Electronics, M. I. T., January 15, 1965, pp. 130-133.
3. J. Woo, "Study of a Highly Ionized Plasma Column in a Strong Magnetic Field," Ph. D. Thesis, Department of Nuclear Engineering, M. I. T., June 1966.

2. A POSSIBLE VERY INTENSE PULSED CONTINUUM X-RAY SOURCE

As part of our general study of intense particle and radiation sources, we have completed a brief feasibility study of a continuum x-ray source. The particular source discussed in this report produces copious radiation in the 25-250 keV energy range in a

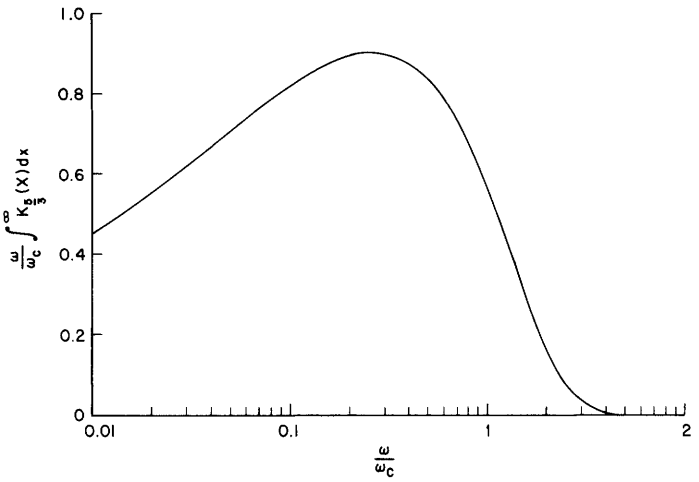

Fig. XXIII-25. Normalized cyclotron radiation spectrum.

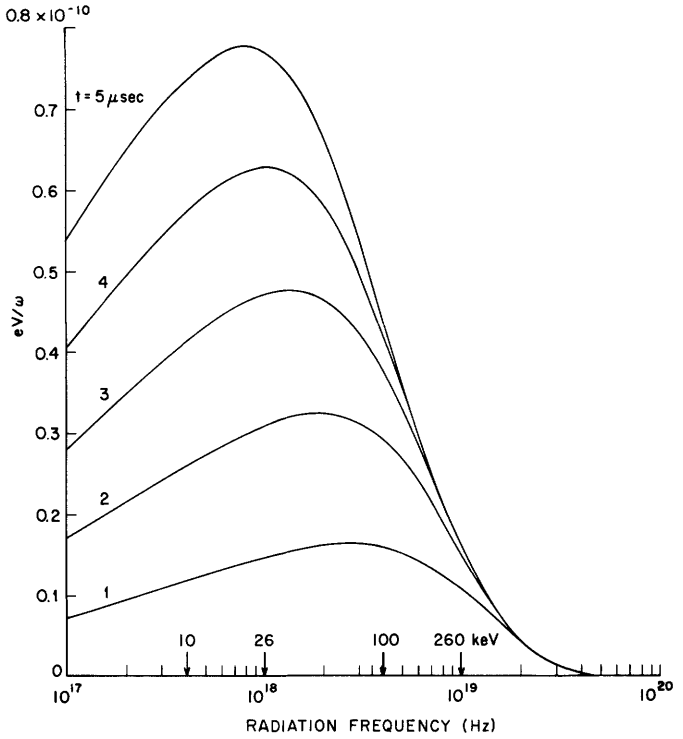

Fig. XXIII-26. Spectral distribution of cyclotron radiation ($t \leq 5.0$ μsec). B = 25 W/m^2, E_o = 2000 MeV.

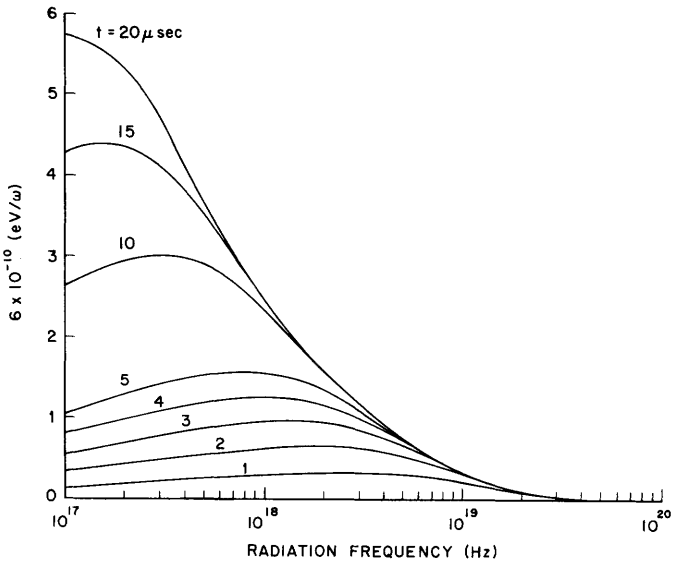

Fig. XXIII-27. Spectral distribution of cyclotron radiation ($t \leq 20.0$ μsec). $B = 25$ W/m^2, $E_o = 2000$ MeV.

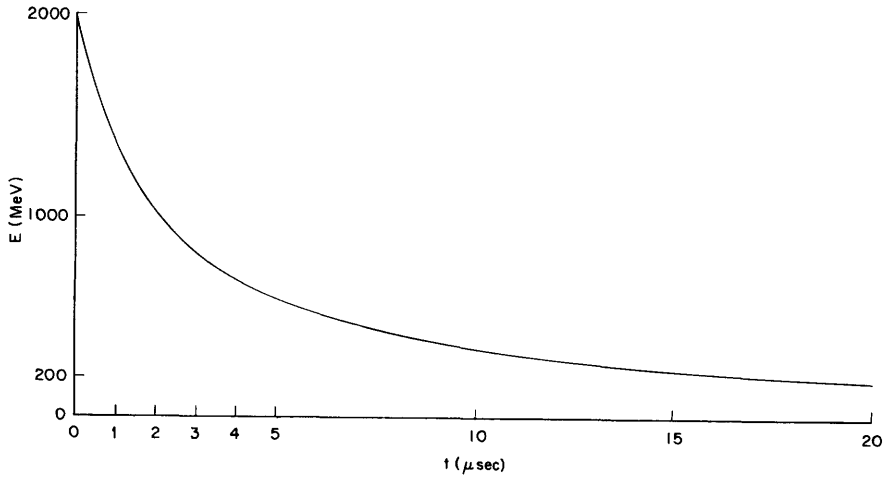

Fig. XXIII-28. Electron energy as a function of time (B = 25 W/m^2).

pulse of ~5-μsec width, but these parameters are subject to considerable variation. Intense x-ray bursts of this sort are typical of those that might be produced, for example, in pulsed controlled fusion reactors.

Relativistic electrons in magnetic fields radiate energy at the cyclotron frequency and its harmonics. The resulting spectrum is nearly flat out to a critical frequency, ω_c, and then falls off very rapidly. The critical frequency is given[1] by

$$\omega_c = 3\gamma^2\left(\frac{c}{\rho}\right), \tag{1}$$

where $\gamma = (1-v^2/c^2)^{-1/2}$, and ρ is the radius of curvature of the electron orbit in the magnetic field. For a characteristic photon energy, $E_c = \hbar\omega_c$, the requisite electron energy is related to the magnetic field, B, by

$$\gamma^2 = \frac{m_o E_c}{3\hbar B}. \tag{2}$$

For E_c = 100 keV, and B = 25 W/m^2, we find that the electron energy is in the neighborhood of 2 GeV and the Larmor radius ≈ 23 cm. The "betatron radiation" is intense for such highly relativistic electrons, and the standard accelerator formulas yield $E/\dot{E} = 2.5 \times 10^{-6}$ sec. Since 2 GeV electron energies are certainly technologically feasible (the Stanford Mk III linac produces 1-GeV electrons, while SLAC yields >20.0 GeV) and 250,000-kG fields are, in principle, attainable, even in large volume on a pulsed basis, we proceed to a more careful calculation.

Consider an electron injected at t = 0 into a uniform constant magnetic field. Schwinger gives, for the total radiated power,

$$P(t) = \frac{2}{3}\omega_o \frac{e^2}{R}\beta^3\left(\frac{E}{m_o c^2}\right)^4 \tag{3}$$

and, for the spectral distribution,

$$P(\omega,t) = \frac{3^{3/2}}{4\pi}\frac{e^2}{R}\left(\frac{E}{m_o c^2}\right)^4 \frac{\omega_o \omega}{\omega_c^2}\int_{\omega/\omega_o}^{\infty} K_{5/3}(\eta)\, d\eta, \tag{4}$$

where $\omega_c = \frac{3}{2}\omega_o\left(\frac{E}{m_o c^2}\right)^3$, $\omega_o = \frac{c}{R}$, $R = \frac{m_o v}{qB}\left(\frac{E}{m_o c^2}\right)$, and it has been assumed that $E \gg m_o c^2$ and $\omega \gg c/R$. Equation 3 may be solved to yield the history of particle energy, and Eq. 4 can be simplified to give the set

$$E(t) = m_o c^2 \coth\left[\frac{2}{3}\frac{ce^2}{m_o c^2}\left(\frac{eB}{m_o c^2}\right)^2 t + \coth^{-1}\left(\frac{E_o}{m_o c^2}\right)\right] \tag{5a}$$

$$P(\omega,t) = \frac{\omega}{\sqrt{3}\,\pi}\frac{e^2}{c}\left[\frac{m_o c^2}{E(t)}\right]\int_{\omega/\omega_c}^{\infty} K_{5/3}(\eta)\,d\eta. \tag{5b}$$

No tabulations of the integral in Eq. 5b were known to us, so it was solved numerically in normalized units (see Fig. XXIII-25) and for the special case of 2-GeV electrons in a 250-kG field (see Fig. XXIII-26). The peak of the radiated spectrum moves down in energy as the electron cools and, as is seen in Fig. XXIII-27, by 10 μsec the radiation is all at energies of less than 25 keV. The total radiated energy per electron follows from Fig. XXIII-28. For the parameters under discussion here, the electrons have radiated 1.4 GeV in 5.0 μsec.

There is no single parameter that is useful for describing source intensity because the radiated spectrum changes with time and with angle measured from the plane of rotation. The total energy/pulse radiated in the 25-250 keV region of the photon spectrum during the first 5 μsec is probably as good a measure as any for evaluating the utility of the source for possible experiments. If the injection pulse is supplied by an electron linac, then the pulse current will be limited by "beam breakup instabilities." The limiting current[2] is given by $I = K(\partial v/\partial z)/L\tau$, where K is an empirical constant depending on the accelerator structure, $\partial v/\partial z$ is the average energy gradient, L is the accelerator length, and τ is the pulse duration.[2] For the Stanford Mk III and for SLAC, $K \approx 2 \times 10^4$ mA for energies measured in MeV and τ measured in microseconds. For an accelerator, 200 meters long, based on the Mk III design, it should be possible to inject approximately $\sim 10^{13}$ electron/pulse. This corresponds to 1.5×10^3 J/pulse in the soft x-ray continuum.

K. Chen, L. M. Lidsky

References

1. J. Schwinger, Phys. Rev. 75, 1912 (1948).
2. R. B. Neal, Physics Today 20, 27 (1967).

XXIII. PLASMAS AND CONTROLLED NUCLEAR FUSION

C. Active Plasma Effects in Solids*

Academic and Research Staff

Prof. A. Bers
Prof. G. Bekefi
Dr. W. M. Manheimer

Graduate Students

E. V. George
C. W. Hartman
D. A. Platts
J. H. Spencer
R. N. Wallace

RESEARCH OBJECTIVES

We intend to study the collective (plasma-type) effects of free carriers in a solid, with particular emphasis on the exploration of unstable modes of oscillation and wave propagation. Our research activity in this area has been evolving during the past three years. Experimental studies have been focused on the microwave emission from n-type InSb bars at 77°K and 4°K with applied electric and magnetic fields. Theoretical studies have been concerned with instabilities of drifted helicons and drifted electron-phonon interactions in a magnetic field. During the coming year we plan the following studies.

1. Microwave Emission from n-Type Indium Antimonide

Indium Antimonide emits microwave noise when it is subjected simultaneously to DC electric and magnetic fields. The cause of the instability that gives rise to this emission is not fully understood. Experiments made at temperatures ranging from 1.2°K to 77°K are now under way, the purpose of which is to determine the frequency and temperature characteristics of the emission as a function of sample size, carrier concentration, and surface quality of the sample.

2. Effect of Contacs on Microwave Emission from InSb

Although the onset of emission is found to be insensitive to surface conditions and contacting procedures, the magnitude of the emission changes when the electric field is reversed. To find out whether the emission comes from the bulk of the material or the contacts, attempts are now being made to observe the microwave emission from ring-shaped samples that have no contacts. The required electric field is induced by a low-frequency time-variant magnetic field that threads the ring.

3. Acoustic Wave Amplification by Electrons Drifting in a Magnetic Field

Our theoretical studies have indicated the possibility of linking the observed microwave emission from InSb with acoustic wave generation by the drifting electrons. We plan to put acoustic transducers onto the surface of the InSb bar to see if we can detect directly the generation of acoustic energy at the onset of microwave emission.

*This work was supported principally by the National Science Foundation (Grant GK-1165).

4. Light Scattering from Unstable Waves

Incoherent scattering of electromagnetic waves from plasma oscillations provides a means of establishing the dispersion characteristics and oscillation amplitudes of the waves in question. A high-power, Q-switched CO_2 laser has been constructed for use as the primary source for the scattering experiments. Work is in progress to scatter from unstable waves generated in Indium Antimonide subjected to DC electric and magnetic fields.

5. Helicon Waves in the Presence of Electron Drift

A helicon wave excited in a plasma can become potentially unstable when the electrons are made to drift through the application of a sufficiently strong DC electric field. Feasibility studies to verify this mode of oscillation experimentally are under way.

A. Bers, G. Bekefi

1. MICROWAVE INSTABILITIES IN A SEMICONDUCTOR SUBJECTED TO DC ELECTRIC AND MAGNETIC FIELDS

We are continuing investigation of the emission of microwave radiation from n-type InSb when a sample is subjected simultaneously to parallel DC magnetic and electric fields.[1]

We have planned to study the emission spectra from 500 MHz up to ~10 GHz. This large frequency range requires the use of a broadband sample holder which has been designed, constructed, and tested. It consists of a center conductor mounted coaxially within an outer conductor. The center conductor is supported by means of a short section of low-loss, dielectric material. The InSb sample is mounted at the end of the coaxial holder in a manner similar to that illustrated in a previous report.[2] The return for the DC current pulse is through the double stub tuner. In all of the measurements reported here this broadband holder was used.

Upon investigating the output emission for a sample 1 mm × 1 mm × 15 mm at 77°K, a spikey behavior similar to that reported previously[1] at 4.2°K was obtained. This is illustrated in Fig. XXIII-29, where the output of the radiometer is displayed on an x-y recorder as a function of the peak voltage applied to the sample. The occurrence of a given spike is a very sensitive function of the precise electric field of the DC pulse (it is a much less sensitive function of the applied magnetic field). Thus, to obtain clear reproducible spikes, great care must be taken to satisfy the following conditions: (a) the DC pulse must be uniform to better than 1% over the duration of the sampling gate; and (b) the electric field must be reproducible within the same accuracy from pulse to pulse over the integration time of the radiometer. In order to increase the resolution of the spike, the IF gate width was reduced from the 2-μsec value previously used[1] to 1/2 μsec. The current pulse was 3 μsec wide at a repetition rate of 200 pulses/sec. This spikey behavior was observed for both a positive and negative polarity

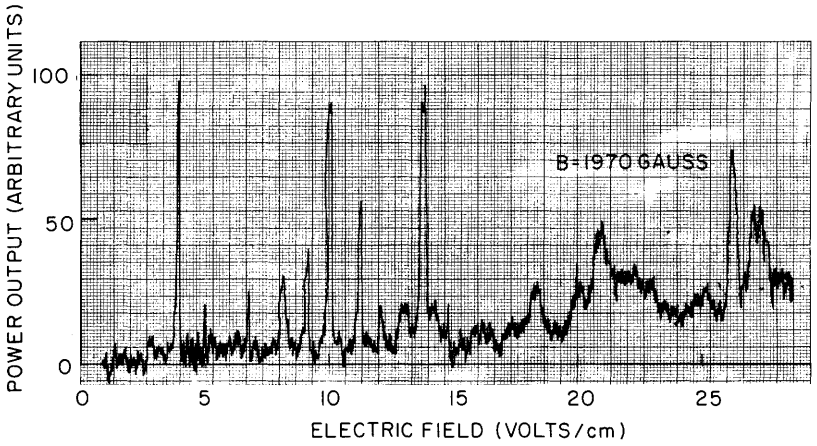

Fig. XXIII-29. Noise-power output as a function of electric field for one value of magnetic field, at 77°K. The observation frequency was 3 GHz.

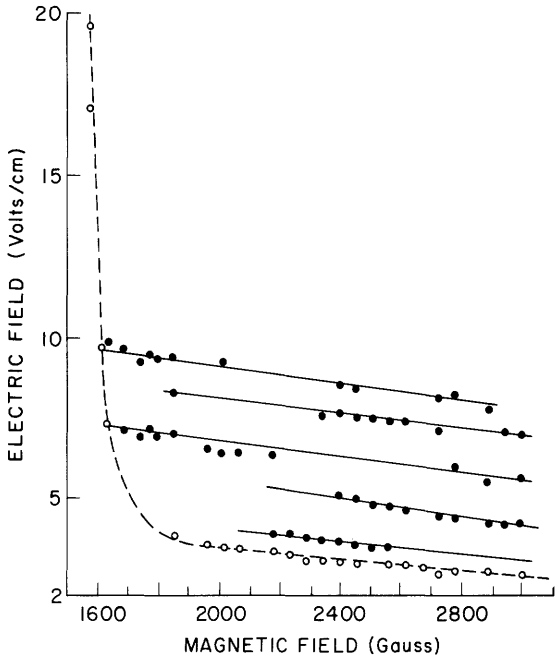

Fig. XXIII-30. Threshold electric field vs threshold magnetic field for spikey microwave emission at 77°K. Observation frequency: 3 GHz.

of the current pulse. It was also observed in samples as short as 7.5 mm.

The dependence of the spikes as a function of the applied DC electric and magnetic fields is illustrated in Fig. XXIII-30. The open circles joined by the dashed line represents the threshold characteristics for the onset of the noise spikes at a fixed frequency of observation equal to 3 GHz. The solid circles and the solid lines illustrate the E_o-B_o

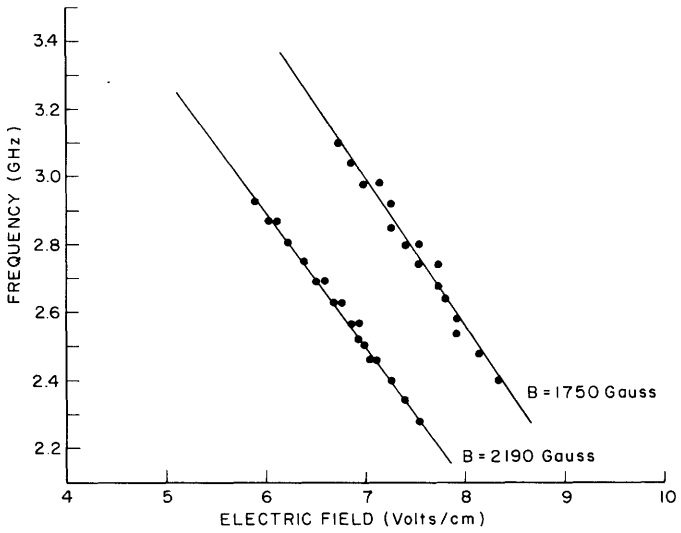

Fig. XXIII-31. Frequency of one microwave spike as a function of electric field for two values of magnetic field at 77°K.

characteristics above threshold of a few prominent spikes.

It is interesting to note that the dashed line appears to trace out the threshold curve for the "continuum" microwave emission previously reported.[1] It is therefore suggested that the previously observed continuum noise is merely a superposition of spikes that were not previously resolved, because of the poor current waveform of the breakdown pulse.

In Fig. XXIII-31 the frequency voltage spectra are plotted for one prominent spike, at two different magnetic field values. It has been observed experimentally that the character of this frequency voltage curve may be different for other spikes, and work is now under way to verify this.

E. V. George

References

1. G. Bekefi and A. Bers, Quarterly Progress Report No. 85, Research Laboratory of Electronics, M.I.T., April 15, 1967, pp. 128-134.
2. Ibid., see Fig. XI-39.

2. INTERACTIONS OF ACOUSTIC WAVES WITH DRIFTING ELECTRONS IN A MAGNETIC FIELD

We have previously studied unstable electron-phonon interactions in a magnetic field, using a Boltzmann-type description for the electrons.[1-3] Such a description

allowed us to look at high frequencies at which the electron's mean-free path was comparable to or larger than an acoustic wavelength. Because of the complexity of such analyses, the evaluation of growth rates and of their dependence upon physical parameters has been carried out for only the simplest geometries of applied electric and magnetic fields.

In this report we return to a simpler description of the electrons, which is valid for lower frequencies at which their mean-free path is short compared with an acoustic wavelength. This simplification allows us to explore various geometries of the applied electric and magnetic fields, and to determine the maximum acoustic amplification as a function of drift velocity, magnetic field, frequency of operation, and so forth.

Electron Plasma System

We assume the electrons to be described by a simple set of transport model equations

$$n\nu m\bar{v} + \nabla(n\kappa T) = ne(\bar{E}+\bar{v}\times\bar{B}) \tag{1}$$

$$\nabla \cdot (n\bar{v}) + \frac{\partial n}{\partial t} = 0, \tag{2}$$

where n is the particle density, ν is the effective collision frequency, m is the effective mass, $\bar{v}$ is the macroscopic velocity, κ is Boltzmann's constant, T is the effective temperature – a constant, e is the electron's charge, and $\bar{E}$ and $\bar{B}$ are, respectively, the electric and magnetic fields. In Eq. 1 it is assumed that $\nu \gg \omega$ and $\nu \gg \bar{q} \cdot \bar{w}$, where ω is the frequency, $\bar{q}$ is the wave vector, and w is the electron's velocity (thermal and/or drift).

In the presence of time-invariant and uniform fields $\bar{E}_o$ and $\bar{B}_o$, and a uniform density n_o, the electrons acquire a drift velocity $\bar{v}_o$, given by the solution of Eq. 1,

$$\bar{v}_o = -\mu\bar{\bar{b}} \cdot \bar{E}_o, \tag{3}$$

where $\mu = -e/m\nu$ is the mobility,

$$\bar{\bar{b}} = \begin{bmatrix} \frac{1}{1+b^2} & \frac{-b}{1+b^2} & 0 \\ \frac{b}{1+b^2} & \frac{1}{1+b^2} & 0 \\ 0 & 0 & 1 \end{bmatrix}, \tag{4}$$

and $b = \mu B_o = \omega_c/\nu$.

Assuming first-order electrostatic ($E_1 = -\nabla\Phi$) perturbations of the form $\exp j(\omega t - \bar{q}\cdot\bar{r})$,

we can determine from Eqs. 1-4 the effective longitudinal conductivity, $\sigma_\ell = -j\omega e n_1/q^2\Phi_1$,

$$\sigma_\ell(\omega,\bar{q}) = \sigma_o \frac{\omega b_\ell}{\omega - \bar{q}\cdot\bar{v}_o - jq^2 b_\ell D}, \tag{5}$$

where $\sigma_o \equiv -e\mu n_o$ is the DC conductivity, $D = \kappa T/m\nu$ is the diffusion constant, and

$$b_\ell = \frac{\bar{q}\cdot\bar{\bar{b}}\cdot\bar{q}}{q^2} = \frac{1 + b^2\cos^2\theta}{1 + b^2}, \tag{6}$$

where θ is the angle between $\bar{q}$ and $\bar{B}_o$.

Longitudinal Electron-Phonon Interaction

We assume that the electrons are coupled to the acoustic wave by piezoelectric and/or deformation potential effects in the solid. Let the effective longitudinal coupling constants be $e_p(C/m^2)$ for piezoelectric coupling, and C_D (volts) for deformation potential coupling. The coupled longitudinal electron-phonon dispersion relation is then

$$\left(\omega^2 - q^2v_s^2\right) K_\ell(\omega,\bar{q}) = q^2v_s^2P^2, \tag{7}$$

where

$$P^2 = \frac{e_p^2}{C\epsilon_L} + q^2\frac{C_D^2\epsilon_L}{Ce^2} \tag{8}$$

$$K_\ell(\omega,\bar{q}) = 1 + \frac{\sigma_\ell(\omega,\bar{q})}{j\omega\epsilon_L} \tag{9}$$

with v_s the sound-wave velocity, C the elastic constant, ϵ_L the lattice dielectric constant, and we have assumed that the sound waves in the absence of the free electrons (that is, for $\sigma_\ell = 0$) are unattenuated. Usually, the coupling is weak ($P^2 \approx 0$), and Eq. 7 can be solved approximately. We expect the electron-phonon instability to be convective, hence let ω be real and $q = q_r + jq_i$. From Eq. 7 we then have approximately

$$q_r \cong \frac{\omega}{v_s} \tag{10}$$

$$q_i \cong -\frac{1}{2}\frac{\omega}{v_s}P^2\,\mathrm{Im}\left[\frac{1}{K_\ell(\omega,\bar{q}_r)}\right]. \tag{11}$$

Using Eqs. 9, and introducing the dielectric relaxation frequency $\omega_o = \sigma_o/\epsilon_L$, we can

write (11) in the form

$$q_i = -\frac{1}{2} P^2 \frac{\omega}{v_s} \frac{\frac{\omega_o}{\omega} \mathrm{Re}\left[\frac{\sigma_\ell(\omega, \bar{q}_r)}{\sigma_o}\right]}{\left|1 - j \frac{\omega_o}{\omega} \frac{\sigma_\ell(\omega, \bar{q}_r)}{\sigma_o}\right|^2}. \tag{12}$$

Equations 10-12 are general; no particular description of the electron plasma system is assumed, that is, $\sigma_\ell(\omega, \bar{q})$. We now assume that $\sigma_\ell(\omega, q)$ is given by Eq. 5. Substituting Eq. 5 in Eq. 12, we finally obtain

$$q_i = \frac{1}{2} P^2 \frac{\omega_o}{v_s} \frac{b_\ell \delta}{\delta^2 + b_\ell^2 \left(\frac{\omega_o}{\omega} + \frac{\omega}{\omega_D}\right)^2}, \tag{13}$$

where

$$\delta = \frac{\bar{q}_r \cdot \bar{v}_o}{\omega} - 1 \tag{14}$$

describes the effective deviation of the drift velocity from the acoustic phase velocity, and $\omega_D = v_s^2/D$ is the diffusion frequency.

Maximum Acoustic Gain Conditions

Equation 13 has a maximum with respect to frequency ω. The frequency for maximum growth is

$$\omega_{max} = \sqrt{\omega_o \omega_D}. \tag{15}$$

To take an example: For n-type InSb at 77°K with $n_o = 2 \times 10^{14}/\mathrm{cm}^3$, $\mu = 5 \times 10^5$ cm^2/volt-sec, $m = 0.013\, m_e$, and $\epsilon_L = 16\epsilon_o$, we find $\omega_o \approx 10^{13}$/sec, $\omega_D \approx 5 \times 10^7$/sec, and $\omega_{max} \approx 2.2 \times 10^{10}$/sec.

The growth rate q_i of Eq. 13 also has a maximum with respect to δ and b_ℓ when

$$\delta^2 = b_\ell^2 \left(\frac{\omega_o}{\omega} + \frac{\omega}{\omega_D}\right)^2. \tag{16}$$

Combining Eqs. 15 and 16, we find

$$\delta = 2 b_\ell \left(\frac{\omega_o}{\omega_D}\right)^{1/2}, \tag{17}$$

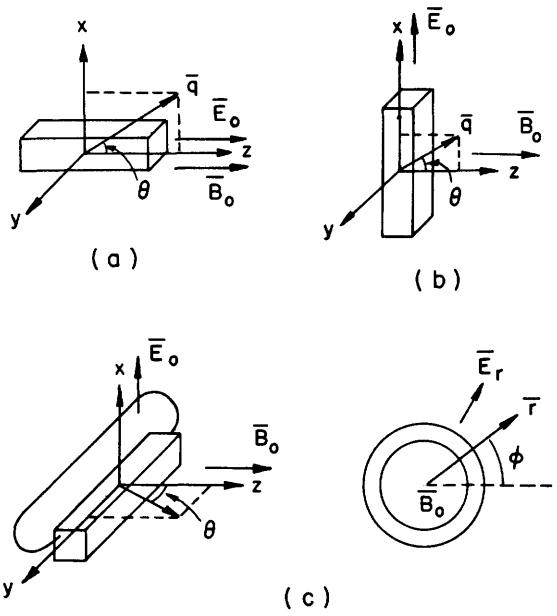

Fig. XXIII-32. Geometries of applied electric and magnetic fields with respect to acoustic wave vector $\bar{q}$.

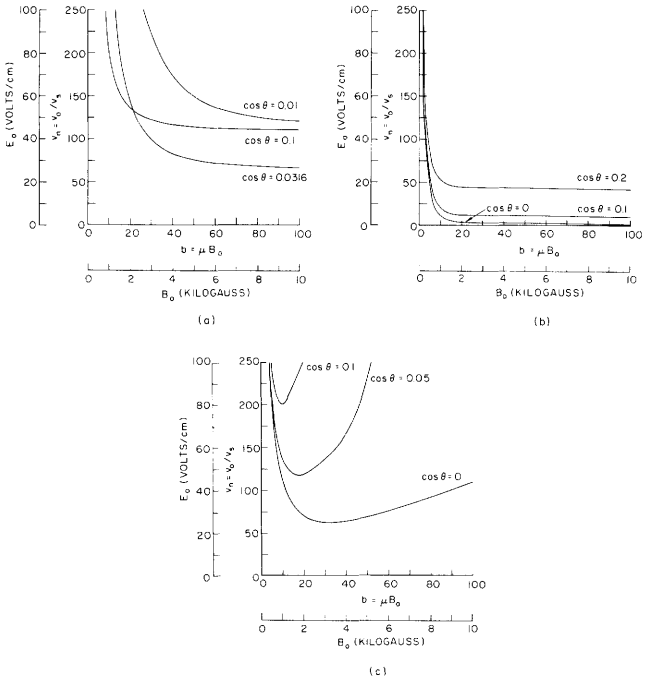

Fig. XXIII-33. Maximum growth rate parameters for the corresponding three cases of Fig. XXIII-32. The values of E_o and B_o are those pertaining to the example of InSb given in the text.

and substituting in (13), we obtain the maximum growth rate

$$(q_i)_{max} = \frac{1}{8} P^2 \frac{\omega_{max}}{v_s}. \tag{18}$$

For InSb parameters used above, with $P^2 = 3.2 \times 10^{-4}$ and $v_s = 4 \times 10^5$ cm/sec,[4] $(q_i)_{max} \approx$ 2.2/cm, that is, approximately 20 db/cm.

The conditions implied by (17) can be evaluated for several geometries of interest. Three such cases are illustrated in Fig. XXIII-32. The maximum growth rate conditions for these three cases have been calculated for $(\omega_o/\omega_D)^{1/2} = 500$, which corresponds to the parameters used above for InSb, and they are plotted in Fig. XXIII-33.

A. Bers

References

1. A. Bers and T. Musha, Quarterly Progress Report No. 79, Research Laboratory of Electronics, M.I.T., October 15, 1965, pp. 99-109.
2. S. R. J. Brueck and A. Bers, Quarterly Progress Report No. 83, Research Laboratory of Electronics, M.I.T., October 15, 1966, pp. 72-76.
3. S. R. J. Brueck, S.M. Thesis, Department of Electrical Engineering, M.I.T., January 1967.
4. K. W. Nill, Ph.D. Thesis, Department of Electrical Engineering, M.I.T., May 1966.